Available online at www.sciencedirect.com
SCIENCE DIRECT®
Carbohydrate Polymers 53 (2003) 15–44
Carbohydrate Polymers
www.elsevier.com/locate/carbpol

Host–guest inclusion complexes between anticancer drugs and β-cyclodextrin: computational studies

M. Fermeglia, M. Ferrone, A. Lodi, S. Pricl*

Computer-aided Systems Laboratory, Department of Chemical, Environmental and Raw Materials Engineering—DICAMP, University of Trieste, Piazzale Europa 1, 34127 Trieste, Italy

Received 13 February 2002; revised 1 October 2002; accepted 16 October 2002

Abstract

In this paper we analyze the possibility of forming host–guest inclusion complexes between β-cyclodextrin (BCD) and several anticancer active principles, characterized by different mechanism of action, by atomistic molecular dynamics simulations. The trajectories of the insertion angles, rotation of the non-polar parts of the drugs inside the macrocycle and other geometrical features give detailed information on the dynamics of the complexes. The relative binding energies in all cases indicate possibilities of formation of inclusion complexes between BCD and the anticancer drugs either in a 1:1 or in a 2:2 stoichiometry.

Keywords: Anticancer drugs; β-Cyclodextrin; Host–guest inclusion compounds; Free energy of binding; Molecular dynamics simulations

1. Introduction

In order to design a drug delivery system (DDS), various kinds of high-performance carrier materials are being developed to deliver the necessary amount of drug to the targeted site for a necessary period of time, both efficiently and precisely. Cyclodextrins (CDs) are potential candidates for such a role, because of their ability to alter physical, chemical and biological properties of guest molecules through the formation of inclusion complexes in both solution and solid state (Hirayama & Uekama, 1999; Szente & Szejtli, 1999). The α-, β- and γ-CDs are the most common natural CDs, consisting of six, seven and eight D-glucopyranose residues, respectively, linked by α-1,4 glycosidic bonds into a macrocycle. Each CD has its own ability to form host–guest inclusion complexes with specific guest molecules, an ability which depends on a proper fit of the guest molecule into the hydrophobic CD cavity. The principal advantages of natural CDs as drug carriers are: (1) a well-defined chemical structure, yielding many potential sites for chemical modification; (2) the availability of CDs of different cavity sizes; (3) low toxicity and low pharmacological activity and (4) the protection of the included drug molecule from biodegradation. The main applications of natural CDs are to enhance solubility, stability and bioavailability of the drug molecules; further, the enhancement of drug activity, selective transfer and/or reduction of side effects can be achieved by means of host–guest complexation (Loftsson & Brewster, 1996; Thompson, 1997; Uekama, Hirayama, & Irie, 1994).

β-Cyclodextrin (BCD) consists of seven D-glucopyranose monomers covalently bound by α-1,4-linkages. From a topological point of view, this macrocycle can be described as a truncated cone, in which the narrow rim (~6.4 Å) bears the primary hydroxyl group whereas the wide rim (~15.4 Å) bears the secondary OH groups. Since no hydroxyl group is present within the toroidal cavity of BCD, this zone of the molecule has a pronounced hydrophobic character. Accordingly, this feature, together with van der Waals forces and hydrogen bonding allow BCD to host small molecules efficiently in aqueous solutions.

Drugs used in the fight against cancer can be divided into four categories, according to their mechanism of action (Holland & Frei, 2000; Katzung, 1998): (1) alkylating agents, (2) RNA/DNA antimetabolites, (3) antimitotic agents and (4) inhibitors of topoisomerases I and II. In

* Corresponding author. Tel.: +39-40-5583-750; fax: +39-40-569-823.
E-mail address: sabrinap@dicamp.units.it (S. Pricl).

0144-8617/03/$ - see front matter © 2003 Elsevier Science Ltd. All rights reserved.
doi:10.1016/S0144-8617(03)00011-0

particular, all alkylating agents exert their cytotoxic effects by transferring their alkyl groups to various cellular constituents. Direct DNA alkylation within the cellular nuclei undoubtedly represent the principal interactions, which lead to cellular death. The main site for DNA alkylation is the N^7 position of guanine, although other moieties, such as N^1 and N^3 of adenine, N^3 of cytosine and O^6 of guanine, are also alkylated to a lesser extent. Such interactions may take place on a single DNA strand, or can have effect on both strands, since the most powerful anticancer of type (1) are bifunctional molecules. Nonetheless, the ultimate cause of cell death related to DNA damage is still not known. Some of the cellular responses produced include cell-cycle arrest, DNA repair and apoptosis or programmed cell death. The nucleophilic groups of proteins, RNA and many other molecules can also be subject to attack by the alkylating agents, although the exact result of these interactions is again not well understood.

RNA/DNA antimetabolites are molecules structurally related to naturally occurring compounds, i.e. vitamins, amino acids or nucleosides. They interfere with the production of nucleic acids by preventing the synthesis of normal nucleoside triphosphates by inhibiting key enzymes and substituting for normal purines or pyrimidines. The final result is a net decrease in DNA or RNA synthesis with consequent interference with cell growth and proliferation.

Based on the notion that some tumor cells may proliferate more rapidly than normal cells, a common strategy for cancer chemotherapy has been to develop drugs that interrupt the cell cycle. A particularly attractive stage of the cell cycle for intervention is mitosis, during which the mitotic spindle (a bipolar apparatus constructed of microtubules) separates the replicated chromosomes. Chromosome attachment to and movement on the spindle is intimately tied to the dynamics of microtubule polymerization and depolymerization. The sister chromatid pairs must maintain a stable attachment to spindle microtubules as the microtubules interconvert between growing and shrinking states. Drugs that perturb microtubule lengthening (polymerization) or shortening (depolymerization) (i.e. antimitotic agents) cause arrest of the cell cycle in mitosis because they perturb the normal microtubule dynamics necessary for chromosome movement.

Topoisomerases inhibitors are drugs, which disrupt the chromosomal dynamics necessary to carry out DNA replication and mitosis. To fit into the nuclei of eukaryotic cells, chromosomal DNA is extensively twisted. The enzyme topoisomerases permit selected regions of DNA to untangle to allow transcription and replication to occur; further, the same biomacromolecules temporarily break DNA, allowing for topological changes, and then reseal the relevant breaks. As a general mechanism of action, the inhibitors stabilize the topoisomerase–DNA complex preventing it from making a topological change. This results in an irreversible double strand break lethal to cells in the S and G_2 phases.

Besides these aspects, unfortunately several are the side effects and the toxicity exerted by this class of anticancer active compounds. In general, they induce systemic toxicity, present direct vesicant consequences and may eventually damage the tissue at the point of parenteral administration. As a rule, toxicity is directly connected to the dosage, and becomes manifest at the level of those tissue characterized by the fastest proliferation rate, such as the bone marrow, the gastrointestinal tract and the gonads. When administered per os, leucopoenia is a typical collateral symptom, unavoidably associated to drug adsorption.

Due to low water solubility, this high toxicity and the plethora of side effects which characterize all anticancer molecules employed so far, we thought that their encapsulation in BCD could be one method to increase their bioavailability and, contemporarily, to limit their deleterious effects. For this reason, we performed a detailed molecular dynamics study focused on (a) modeling of the molecular interactions of BCD molecule with five anticancer drugs belonging to the different classes plus one recently developed drug and (b) evaluation of the interaction energies, the free energies of binding, and analysis of the energetic contribution in host–guest inclusion compounds between BCD and the antineoplastic active principles considered. In details, the six drugs considered are the following: Pipobroman (piperazine, 1,4-bis(3-bromo)-1-oxopropyl), NSC 25154,), Melphalan (L-phenylalanine, 4-[bis(2-chloroehtyl)amino], NSC 8806), Acivicin (5-isoxazoleacetic acid, alpha-amino-3-chloro-4,5-dihydro-, [S-(R*,R*)]-(9CI), NSC 163501), 7-Chlorocamptothecin (1H-Pyrano[3′,4′:6,7]indolizino[1,2-b]quinoline-3,14(4H,12H)-dione, 11-chloro-4-ethyl-4-hydroxy-, (S)-, NSC 249910), Thicolchicine (thiocolchicine, 3-demethyl-acetamide, N-[5,6,7,9-tetrahydro-3-hydroxy-1,2-dimethoxy-10-(methyl thio)-, NSC 361792) and Hexahydro-TMC69 ([5Z(E,E)]-1,4-dihydroxy-5-phenyl-3-[tetrahydro3-methyl-5-(6-methyl)-2,4-octane]-2H-pyran-2-yl]-2(1H)-pyridinone).

Pipobroman and Melphalan belong to class (1). The former is currently used in chronic myelocytic leukemia, whereas Melphalan is mostly employed in the treatment of multiple myeloma, although it is also used against breast cancer, Ewing's sarcoma, malignant melanoma, neuroblastoma and ovarian cancer. Acivicin (class 2), is a potent inhibitor of CTP and guanine monophosphate synthetases, partially inhibits FGAM synthetase and exerts a potent inhibitory action of carbamyl phosphate synthetase II, the glutamine-hydrolyzing first enzyme of de novo pyrimidine biosynthesis. Although Acivicin is an investigational drug not yet approved by the FDA but available through the National Cancer Institutes, it has shown activity in preliminary human testing against non-small cell lung cancer, colon and stomach cancer. Unique classes of natural product anticancer drugs have been derived from plants. As

distinct from those agents derived from bacterial and fungal sources, these plant products, as represented for instance by the *Vinca* and *Colchium* alkaloids, do not target DNA. Rather, among the many biological effects seen after exposure of cells and tissues to these agents are disruption of microtubules, inhibition of synthesis of proteins and nucleic acids, elevation of oxidized glutathione, alteration of lipid metabolism and elevation of cAMP. Despite all these biochemical actions, the antineoplastic activity of these drugs is usually attributed to their ability to disrupt microtubules, causing the dissolution of the mitotic spindles and metaphase arrest in dividing cells. Accordingly, they belong to class 3. In particular, Thiocolchicine and other *Vinca* alkaloids have been introduced into the clinical treatment of cancer in combination therapies which extends beyond the spectrum of cancers for which definitive activity has been demonstrated, and include both Hodgkin and non-Hodgkin lymphoma, rhabdomyosarcoma of childhood, neuroblastoma and nephroblastoma. Camptothecin (class 4), a five-ringed heterocyclic alkaloid, is a topoisomerase I poison that does not bind DNA in the absence of the enzyme. Certain substitutions in the A ring, such as 7-Chlorocamptothecin, generally augment topoisomerase poisoning, presumably by increasing drug binding to the topoisomerase I-DNA cleavage complex. Depending on the different substitutions, this class of compounds, although highly toxic, is employed in the treatment of ovarian cancer, small cell and non-small cell lung cancer, acute myelocytic leukemia and myelodysplastic syndromes. Finally, we considered Hexahydro-TMC69, a new antitumor antibiotic possessing activity against cdc25A phosphatase and isolated from the fermentation broth of a mitosporic fungus (Kohno et al., 2001). This molecules showed cytotoxic activity against various tumor cell lines and induced significant prolongation of survival time of mice transplanted with B16 melanoma as well as P388 leukemia.

2. Calculations

All simulations were run on a Silicon Graphics Origin 200 and performed by using AMBER 6.0 (Case et al., 1999; Pearlman et al., 1995) *Cerius*^{2} (v. 4.2, Accelrys, San Diego, USA), Discover (v. 2000, Accelrys, San Diego, USA) and in-house developed codes (stand-alone and add-on to the commercial software).

The starting structure of BCD was its crystallographic geometry (Betzel, Saenger, Hingerty, & Brown, 1984). Missing hydrogens were added with the PARSE module of the AMBER 6.0 package. The all-atom force field (FF) parameters set by Cornell et al. (1995) (in *parm94.dat* file of the AMBER 6.0 code) was applied for cyclodextrin relaxation. The primary cutoff distance for non-bonded interaction was set to 12 Å, the cutoff taper for the Coulomb and van der Waals interactions were 1.2 and 2, respectively. The GB/SA continuum solvation model (Jayaram, Sprous, & Beveridge, 1998; Weiser, Shenkin, & Still, 1999) was used to mimic a water environment in the first series of simulations. Geometry refinement was carried out using the SANDER module via a combined steepest descent–conjugate gradient algorithm, using as a convergence criterion for the energy gradient the root-mean-square (RMS) of the Cartesian elements of the gradient equal to 10^{-4} kcal/(mol Å). As expected, no relevant structural changes were detected upon relaxation, and a good agreement with the experimental geometry was verified (Jaime, Ridondo, Sanchez-Ferrando, & Virgili, 1990). Fig. 1 shows a stereo view of the BCD structure thus obtained.

The accurate model structures for the anticancer active compounds were generated using the 3D sketcher tool of *Cerius*^{2}. All the molecules were subjected to an initial energy minimization using Discover, using a convergence criterion of 10^{-4} kcal/(mol Å). The conformational search was carried out using a combined molecular mechanics/-molecular dynamics simulated annealing (MDSA) protocol

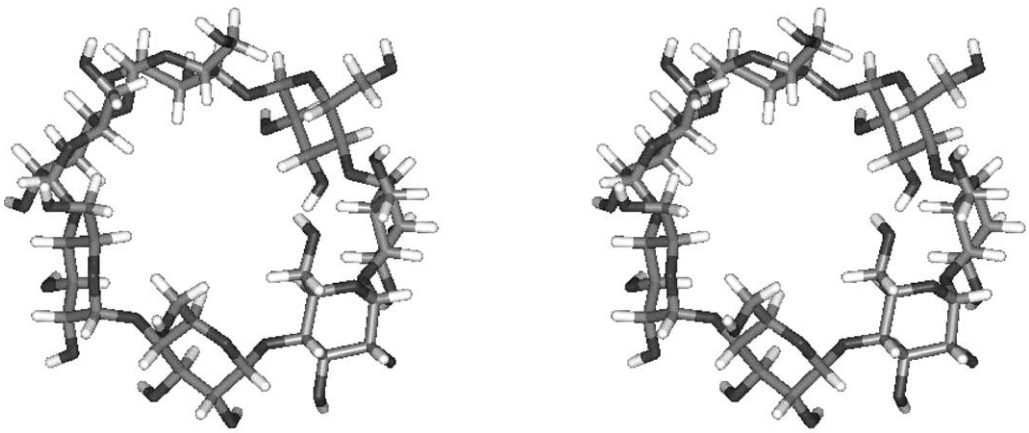

Fig. 1. Stereo view of the relaxed structure of BCD.

(Fermeglia & Pricl, 1999). Accordingly, the relaxed structures were subjected to five repeated temperature cycles (from 310 to 1000 K and back) using constant volume/constant temperature (NVT) MD conditions. At the end of each annealing cycle, the structures were again energy minimized to converge below 10^{-4} kcal/(mol Å), and only the structures corresponding to the minimum energy were used for further modeling. The electrostatic charges for the geometrically optimized drug molecules were obtained by restrained electrostatic potential fitting (Bayly, Cieplak, Cornell, & Kollman, 1993), and the electrostatic potentials were produced by single-point quantum mechanical calculations at the Hartree–Fock level with a 6-31G* basis set. All ab initio calculations were carried out with *DMol*[3] (Delley, 1990), as implemented in the *Cerius*[2] modeling suite.

The inclusion complexes formed between BCD and the drugs were built and refined by Monte Carlo (MC) docking simulations. For this purpose, the host and guest molecules were positioned in the neighborhood with a distance of 10 Å. MC docking started by conjugate gradient energy minimization of this initial configuration for 50 iterations; the resulting structure was then selected as the first frame. Trials to a new configuration were accomplished by changing the position, orientation and/or conformation of the drugs. In this process, the guest molecules could take translational movements along all three Cartesian axes (maximum 7 Å), and the dihedral angles could rotate to a maximum value of 180° for conformational flexibility. Thus, 9 degrees of freedom were present for this system. Each cycle began with a random change of up to 5 degrees of freedom among the 9 possible. If the energy of the resulting configuration was within 1000 kcal/mol from the last accepted one, it was subjected to 50 iterations of conjugate gradient energy minimization. The energy tolerance of 1000 kcal/mol was imposed to avoid significant overlap of the van der Waals radii in the random search. After the energy minimization, acceptance was determined by the following two criteria: (1) an energy check with the Metropolis criteria at 310 K (Metropolis, Rosenbluth, Rosenbluth, & Teller, 1953) and (2) an RMS displacement (RMSD) check, which compared the RMSD of the new configuration against those accepted so far. Configurations within 0.1 A RMSD of pre-existing ones were discarded to avoid accepting similar configurations. The MC docking simulations continued until the complete energy convergence. Each of the best structures resulting from the previous docking procedure was energy minimized, following the minimization protocol described above for the isolated BCD molecule.

The energetic and conformational details of the isolated drug and BCD structures, and the relevant inclusion complexes at the standard body temperature of 310 K were obtained by performing MD simulations under isochoric/isothermal (NVT) conditions. Each molecular dynamics run was started by assigning initial velocity for the atoms according to a Boltzmann distribution at $2 \times T$. Temperature was controlled via weak coupling to a temperature bath (Berendsen, Postma, van Gunsteren, DiNola, & Haak, 1984), with coupling constant $\tau_T = 0.01$ ps. The Newton molecular equations of motion were solved by the Verlet leapfrog algorithm (Verlet, 1967), using an integration step of 1 fs.

Each MD simulation consisted in a system equilibration phase, during which the equilibration process was followed by monitoring the behavior of both kinetic and potential energy, and a successive data collection phase. Almost in all cases, the energy components have ceased to show a systematic drift and have started to oscillate about steady mean values around 50 ps. Accordingly, equilibration phases longer than 100 ps (i.e. 100,000 MD steps with time step = 1 fs) and data acquisition runs longer than 500 ps were judged not necessary to enhance data accuracy.

In all cases, the complexation energies were calculated from the equilibrium molecular dynamics energy components of the non-bonded interactions for the BCD/drug complex $(E_{\text{drug/BCD}})_{\text{NB}}$, the BCD $(E_{\text{BCD}})_{\text{NB}}$ and the drug $(E_{\text{drug}})_{\text{NB}}$ using the following relationship:

$$(\Delta E_{1:1})_{\text{NB}} = (E_{\text{drug/BCD}})_{\text{NB}} - (E_{\text{BCD}})_{\text{NB}} - (E_{\text{drug}})_{\text{NB}} \qquad (1)$$

where $(\Delta E_{1:1})_{\text{NB}}$ is the complexation energy for a given drug inside the BCD cavity in a complex of 1:1 stoichiometry.

Since fairly big molecular dimensions characterized some of the active principles considered, we also analyzed theoretically the stabilization process when these drugs formed complexes of 2:1 stoichiometry starting from simple 1:1 association instead of three isolated molecules, as we assumed the former as the most probable occurrence in a solution with an excess of BCD. In this case, the energy change accompanying the formation of a 2:1 complex was obtained as:

$$(\Delta E_{2:1})_{\text{NB}} = (E_{\text{drug/BCD}})_{\text{NB}} - 2(E_{\text{BCD}})_{\text{NB}} - (E_{\text{drug}})_{\text{NB}} \qquad (2)$$

where $(\Delta E_{2:1})_{\text{NB}}$ denotes the energy of the double complex and the others as above.

With the exception of Pipobroman, all antitumor drugs considered were characterized by a molecular asymmetry; accordingly, two possible orientations in the complex were considered with respect to the different OH functionalities of the BCD. For simplicity, the orientation in which the most characteristic functional group featured by the drug pointed toward the primary hydroxyl rim of the BCD cavity was called *OH prim*, while the other in which the same functional group points towards the secondary hydroxyl rim of the cyclodextrin cavity was named *OH sec*.

Recently, a new computational approach, termed molecular mechanics-Poisson–Boltzmann surface area (MM-PBSA) has shown great promise in its ability to describe the free energy of molecular systems (Srinivasan, Cheatham, Cieplak, Kollman, & Case, 1998). This algorithm combines explicit solvent molecular dynamics simulations with implicit solvation models, Poisson–Boltzmann (PB)

analysis (Gilson & Honig, 1988; Honig & Nicholls, 1995) and non-polar solvation free energy calculations (Sanner, Olson, & Spehner, 1996) to estimate free energies. A set of 'snapshots' along an MD trajectory, which for the highest accuracy is carried out using a periodic box of water molecules and the particle mesh Ewald method (see below) to represent long-range electrostatics, is saved as representative conformations of a molecular complex. When this set of structures is postprocessed, the water molecules are removed and replaced by a continuum solvent model. The free energy of the macromolecular complex consists of the molecular mechanics potential energy of the solute, the solvation free energy, and a solute entropy term. The solvation free energy is further composed of an electrostatic or polar portion, obtained by solving the PB equation, and a non-polar solvation contribution associated with cavity formation in the solvent as well as van der Waals interactions between the solute and solvent. The entropic contribution to the free energy of binding can be finally estimated by normal mode analysis.

For the calculation of the binding free energy of BCD and the six anticancer drugs considered in water, the best energy configuration of each complex resulting from the previous work was solvated by a cubic box of TIP3P water molecules (Jorgensen, Chandrasekhar, Madura, Impey, & Klein, 1983), extending at least 10 Å in each direction from the solute. All water molecules of which the oxygen atom was within 2.3 Å of a non-hydrogen BCD atom were removed. The periodic boundary conditions at a constant pressure of 1 atm were applied, and long-range non-bonded van der Waals interactions were truncated by using a 8 Å residue-based cutoff. The particle mesh Ewald (PME) method (Darden, York, & Pedersen, 1993) was used to treat the long-range electrostatics. Unfavorable interactions within the structures were relieved with steepest descent followed by conjugate gradient energy minimization until the RMS of the elements in the gradient vector was less than 10^{-4} kcal/(mol Å). Each system was gradually heated to 310 K in three intervals, allowing a 5 ps interval per each 100 K, and then equilibrated for 25 ps at 310 K, followed by 2.5 ns of data collection runs. An integration time step of 2 fs has been used with constant temperature, being the temperature maintained at a constant value by the Berendsen coupling algorithm (Berendsen et al., 1984), with separate solute–solvent and solvent–solvent coupling. A total of 2500 snapshots were saved during data collection period, one snapshot per each 1 ps of MD simulation.

The binding free energy ΔG_{bind} of each complex in water was calculated according to the procedure proposed by Srinivasan et al. (1998), and will be briefly described below. According to this method, ΔG_{bind} is calculated as:

$$\Delta G_{\text{bind}} = \Delta G_{\text{MM}} + \Delta G_{\text{sol}}^{\text{C}} - \Delta G_{\text{sol}}^{\text{D}} - \Delta G_{\text{sol}}^{\text{BCD}} - T\Delta S \qquad (3)$$

where ΔG_{MM} is the interaction energy between the drug and the BCD, $\Delta G_{\text{sol}}^{\text{C}}$, $\Delta G_{\text{sol}}^{\text{D}}$ and $\Delta G_{\text{sol}}^{\text{BCD}}$ are the solvation free energy for the complex, the drug and the β-cyclodextrin, respectively, and $-T\Delta S$ is the conformational entropy contribution to the binding. All energetic analysis was done for only a single MD trajectory of the drug/BCD complex considered, with unbound BCD and drug snapshots taken from the snapshots of that trajectory.

ΔG_{MM} can be obtained from the molecular mechanics (MM) interaction energies as:

$$\Delta G_{\text{MM}} = \Delta G_{\text{int}}^{\text{val}} + \Delta G_{\text{int}}^{\text{ele}} + \Delta G_{\text{int}}^{\text{vdW}} \qquad (4)$$

where $\Delta G_{\text{int}}^{\text{val}}$, $\Delta G_{\text{int}}^{\text{ele}}$ and $\Delta G_{\text{int}}^{\text{vdW}}$ are the valence, electrostatic and van der Waals contributions to the interaction energy between the guest and the host. In our case, these quantities were calculated with the *anal* and *carnal* modules from the AMBER 6.0 suite, by applying the infinite cutoffs for all interactions.

The total solvation energy, ΔG_{sol}, is divided in two parts: the electrostatic contribution, $\Delta G_{\text{sol}}^{\text{ele}}$, and the non-polar term, $\Delta G_{\text{sol}}^{\text{np}}$:

$$\Delta G_{\text{sol}} = \Delta G_{\text{sol}}^{\text{ele}} + \Delta G_{\text{sol}}^{\text{np}} \qquad (5)$$

The polar solvation process is equivalent to the transfer of a molecule from one medium with dielectric constant equal to that of the interior of the molecule to another medium with dielectric constant equal to that of the exterior of the molecule. This term yields the free energies because it corresponds to the work done to reversibly change the solute, and it is a polarization free energy because the work goes to the polarization of the solvent. The polar component of ΔG_{sol} was evaluated using the PB approach (Sharp & Honig, 1990). This procedure involves using a continuum solvent model, which represents the solute as a low dielectric medium (i.e. of dielectric constant $\varepsilon = 1$) with embedded charges and the solvent as a high dielectric medium ($\varepsilon = 80$) with no salt. All atomic charges were taken from the Cornell et al. (1995) force field, since these are consistent with the MM energy calculations. However, as suggested by Chong, Duan, Wang, Massova, and Kollman (1999), the atomic radii were taken from the PARSE parameter set (Sitkoff, Sharp, & Honig, 1994) instead of the *parm94* FF set because of the small size of hydrogens in the latter. The dielectric boundary is the contact surface between the radii of the solute and the radius (1.4 Å) of a water molecule. The numerical solution of the linearized PB equations were solved on a cubic lattice by using the iterative finite-difference method implemented in the *DelPhi* software package (Gilson, Sharp, & Honig, 1987). The grid size used was 0.5 Å. Potentials at the boundaries of the finite-difference lattice were set to the sum of the Debye–Hückel potentials.

The non-polar solvation includes cavity creation in water and van der Waals interactions between the modeled non-polar molecule and water molecules. This can be imagined as transferring a non-polar molecule with the shape of the considered system from vacuum to water. This transfer

energy ΔG_{sol}^{np} was calculated from the following equation (Sitkoff et al., 1994):

$$\Delta G_{sol}^{np} = \gamma SA + b \quad (6)$$

in which $\gamma = 0.00542$ kcal/Å^2, $b = 0.92$ kcal/mol, and SA is the solvent-accessible surface estimated using a modified version of the so-called Connolly dot surfaces algorithm (Connolly, 1983, 1985), based on semi-empirical molecular orbital calculations (Fermeglia & Pricl, 1999).

The continuum solvation models discussed above provide estimates of the free energies of solvation, i.e. they implicitly incorporate averages over the solvent degrees of freedom. To complete the estimates of the free energy of binding, we must also determine the entropy components arising from solute degrees of freedom. This in general can be a difficult problem, especially if the magnitude of solute fluctuations is significantly different from one conformational well to another. In our case, the solute entropic contributions were based on the equilibrated structures without water molecules, were estimated using the *nmode* module from AMBER, which involves a harmonic approximation to the normal modes and standard (quantum) formulas, and were determined for each snapshots of the MD trajectories. All minimizations and normal modes calculations were performed with a distance-dependent dielectric ($\varepsilon = 4r_{ij}$, where r_{ij} is the distance between ith and jth atoms) to mimic solvent screening. Steepest descent followed by conjugate gradient minimizations was carried out with a non-bonded cutoff of 15 Å, using as a convergence criterion for the energy gradient the RMS of the Cartesian elements of the gradient less then 10^{-4} kcal/(mol Å). The structures were further minimized with no cutoff for non-bonded interactions by using conjugate gradient and then Newton–Raphson minimizations, until the RMS of the element in the gradient vector was less 10^{-5} kcal/(mol Å). The normal mode analysis was then carried out with no cutoff for non-bonded interactions.

3. Results and discussion

3.1. 1:1 Complexation in the absence of explicit water solvent

The energy-minimized structure of the BCD forms a ring with an inner diameter of about 11.8 Å and a height of about 5.7 Å. These dimensions determine the size of the host cavity. Thus, BCD can accommodate guest molecules with a diameter up to approximately 4.0–5.0 Å, assuming that a close contact of the molecular surfaces of the host and guest molecules sets a limit on the guest molecule size. Accordingly, all the anticancer molecules we considered present parts that are small enough to easily fit into the BCD ring cavity.

During the MD simulation, the isolated BCD molecular structure is slightly deformed, with the primary OH groups mostly rotated towards the interior of the cavity. The secondary hydroxyl groups at the wider rim of the BCD cavity are aligned in an intramolecular hydrogen-bonding pattern (H-bond distance in the range 1.7–2.4 Å, with average dynamic length ADL = 2.09 Å, cutoff for H-bond set to 3 Å) with the neighboring hydroxyl arranged in a cyclic assembly, whose presence characterizes the entire simulation run. Indeed, the formation of a H-bonded rim of secondary OH groups does not necessitate a highly symmetrical BCD conformation, as the two types of hydrogen bonds, *flip* or *flop*, are equally feasible (Mayer & Köhler, 1996). Flip and flop denote H-bonds in which the 2′ or 3′ hydroxyl group, respectively, is the proton donor. During the course of our simulation, no preferential formation of only flip or only flop bonds is observed, and both species are present in the BCD molecule. The breaking of symmetry, which accompanies the BCD dynamics, is in accordance with previous observations (Manunza, Deiana, Pintore, Delogu, & Gessa, 1997; Mayer & Köhler, 1996) and can be quantified by measuring the average distances between neighboring glycosidic oxygen atoms (O_g) calculated over the entire simulation. These are reported in > Table 1. Since in the symmetric model, as obtained from the MM relaxation procedure from the crystallographic data, the mean distances between the O_g atoms from glucose residue i to residue $i + 1$ is about 4.59 Å, and between glucose residue i and residue $i + 2$ is approximately 8.26 Å, Table 1 gives an indication of the extent of the BCD deformation.

In the case of the host–guest complexes, the pathway of MC docking simulations showed a general tendency of inclusion complex formation and lowering interaction energies for all drug considered with BCD. For each compound, the MC process can be divided into three main phases. In an initial phase (up to ~trial 1000), the interaction energies exhibited a fairly rapid decrease, as the drug draws near and in contact with the BCD. In the central phase (up to ~4000 trials), the interaction energies showed a much less steep derivative, as the molecular host is searching for favorable conformations within the hydrophobic cavity. During the last, equilibrium phase, the interaction energies fluctuated around a mean, stable value; accordingly, as explained in Section 2, the lowest

Table 1
Average distances (in Å) between neighboring glycosidic oxygen atoms (O_g) calculated over a set of 500 configurations from the dynamics trajectory of isolated BCD at 310 K (for further explanations, see text)

Glucose residue number	Distance between Ri and R$i + 1$	Distance between Ri and R$i + 2$
R1	4.38	7.57
R2	4.45	7.95
R3	4.32	8.00
R4	4.33	7.73
R5	4.46	7.67
R6	4.38	8.06
R7	4.33	7.86
Average	4.38	7.84

Table 2
Computed free drug energy, complexation energies $(\Delta E_{1:1})_{NB}$ and individual non-bonded complexation energy components obtained from MD calculations in the absence of explicit water solvent at 310 K for all the 1:1 complexes considered. All values are in kJ/mol

Guest	$(E_{drug})_{NB}$	$(\Delta E_{1:1})_{NB}$	$\Delta E^{d}_{1:1}$	$\Delta E^{r}_{1:1}$	$\Delta E^{coul}_{1:1}$
Pipobroman	37.61	−92.38	−231.04	140.42	−1.76
Melphalan F *OH prim*	52.30	−95.48	−269.12	178.07	−4.44
Melphalan F *OH sec*	52.30	−98.83	−241.54	147.28	−4.56
Acivicin Cl *OH prim*	38.45	−71.09	−189.62	122.47	−3.97
Acivicin Cl *OH sec*	38.45	−79.08	−174.64	97.28	−1.72
7-Chlorocampthotecin Ethyl *OH prim*	72.72	−120.67	−318.07	203.76	−6.36
7-Chlorocampthotecin Ethyl *OH sec*	72.72	−122.59	−308.82	188.74	−2.51
Thiocolchicine S *OH prim*	43.14	−120.16	−296.86	176.23	0.46
Thiocolchicine S *OH sec*	43.14	−110.63	−298.82	190.83	−2.59
6H-TMC 69 Octyl *OH prim*	81.13	−122.09	−338.53	217.32	−0.84
6H-TMC 69 Octyl *OH sec*	81.13	−104.27	−275.94	169.41	2.22

All standard deviations (not reported for clarity) were of the order of one tenth of kJ/mol.

energy configuration in this ensemble was then selected and further optimized via MM.

On each optimized host–guest structure, as well as on the single, isolated components, MD simulations were carried out at 310 K in order to obtain information on the energetic of the complex formation. Table 2 reports the computed complexation energies $(\Delta E_{complex1:1})_{NB}$ and the individual contribution of the non-bonded energy components (i.e. the van der Waals dispersive (d) and repulsive (r) terms, and the Coulombic part (coul)) to this quantity obtained from MD calculations for all the cases considered. The corresponding values for the isolated BCD molecule are $(E_{BCD})_{NB} = 227.94$ kJ/mol, $E^{d}_{BCD} = -1113.45$ kJ/mol, $E^{r}_{BCD} = 1213.15$ kJ/mol and $E^{coul}_{BCD} = 128.24$ kJ/mol, respectively. The negative energy changes upon complexation indicates that all drugs could, in principle, form stable complexes with BCD under conditions such as those considered here; further, the magnitude of these values is reasonable for non-bonded supramolecular complexation, and is in agreement with other similar studies (Choi, Yang, Kim, & Jung, 2000; Grigera, Caffarena, & de Rosa, 1998; Ivanov and Jaime, 1996; Jiang, Sun, Shen, Shi, & Lai, 2000; Miertuš et al., 1999a,b; Sanchez-Ruiz, Ramos, & Jaime, 1998). In general, the van der Waals energy stabilization upon complexation is estimated to be in the range 67–121 kJ/mol. In fact, the real driving forces for the inclusion complexation of the BCD and the guest drugs depend, as discussed above, on the intermolecular interactions between the host and the guest and, due to the relatively low polar character of the drugs considered (see below), van der Waals interactions seem to be the main responsible for the final geometry.

3.1.1. BCD–Pipobroman

The first drug considered, Pipobroman, should give stable inclusion complexes with BCD in the gas phase, as indicated by its fairly large negative value of $(\Delta E_{1:1})_{NB}$ (−92.4 kJ/mol, see Table 2). Fig. 2 reports, as an example, a model of the equilibrium structure of the Pipobroman/BCD complex after 400 ps simulation time. It shows that the molecule is set at the center of the BCD cavity: the pyranose rings of the cyclodextrin thus surround the cyclic part of the drug, giving rise to hydrophobic interactions, while the oxygen atoms are wrapped in the OH groups of both BCD cavity openings. Further, whilst the H-bond network between the secondary OH groups does not seem to be affected by the presence of the drug, the simulation reveals the formation of a persistent H-bond between the oxygen atom of the carbonyl group of Pipobroman and the OH groups of the narrower rim, characterized by an average dynamic length (ADL) of 2.5(±0.2) Å.

As concerns the contribution of the single non-bonded component of the potential energy to the complex stabilization, the values reported in Table 2 for Pipobroman indicate a substantial contribution from van der Waals forces (−90.63 kJ/mol) with respect to the Coulombic attractions (−1.76 kJ/mol). The center-of-mass average distance between the BCD and the drug molecule is approximately 1.2 Å, indicating that Pipobroman is deeply inserted in the cavity of BCD; this provides suitable close contacts and, thus, overall favorable dispersive interactions between host and guest. In the case of electrostatic forces, the low electrostatic stabilization energy can be easily justified considering the sum of the dipole moments of the host and the gust in the complexes as well as their relative orientation. Thus, in Table 3 we present the calculated data for the dipole–dipole interactions between the BCD and all active drugs. In the case of Pipobroman, the corresponding $\Delta E^{coul}_{1:1}$ reported in Table 2 can be attributed both to the low dipole moment of this active principle ($\mu = 2.55$ D) and to the average angle of interaction with the BCD dipole moment of 105°, which is good but still far from its optimum value (i.e. 180° (see Table 3)) (Fermeglia & Pricl, 2001). As expected, the inclusion of this guest molecule is not accompanied by a sensible increase of the energy for valence bond and angle deformations, and torsional displacements. The overall contribution from all these energy terms is a stabilization of 3.6 kJ/mol.

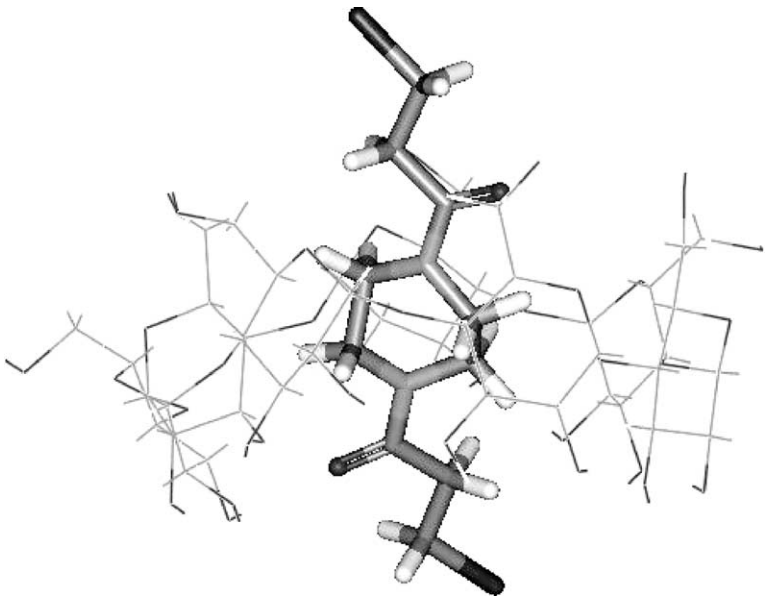

Fig. 2. View of the equilibrium structure of the BCD–Pipobroman complex after 400 ps of MD simulation.

In order to follow the structure and dynamics of this complex in more details, we have identified an angle—the tilt angle φ—defined as the angle formed between the piperazine ring of the drug and the list-squares plane of the BCD. This angle thus describes the orientation of the ring with respect to the central axis of the BCD. In the case of Pipobroman, the value of the tilt angle φ may change as far as 25° (16° on average) out of the parallel alignment with the BCD axis, which is an indication that the drug is inserted only relatively freely in his host cavity. Indeed, the analysis of the molecular models of the corresponding dynamics trajectory reveals that the H-bond between the carbonyl group of Pipobroman and one primary OH group of BCD persists during the whole simulation run, thus keeping the polar group, and hence the entire molecule, in a rather fixed position.

Table 3
Dipole moments μ (D) of the anticancer drugs in the complexes, and average angle of interaction (deg) between the drugs and the BCD in the host–guest complexes obtained from MD simulations in the absence of explicit water solvent at 310 K

Anticancer drug	μ	Angle$_{\mu_{(host/guest)}}$
Pipobroman	2.55	105
Melphalan F *OH prim*	2.73	119
Melphalan F *OH sec*	2.81	116
Acivicin Cl *OH prim*	5.95	134
Acivicin Cl *OH sec*	5.85	78
7-Chlorocampthotecin Ethyl *OH prim*	4.89	96
7-Chlorocampthotecin Ethyl *OH sec*	4.61	114
Thiocolchicine S *OH prim*	2.18	90
Thiocolchicine S *OH sec*	2.78	108
6H-TMC 69 Octyl *OH prim*	2.20	115
6H-TMC 69 Octyl *OH sec*	3.01	106

3.1.2. BCD–Melphalan

The second drug considered is Melphalan. A straight comparison of both possible mode of insertion of this drug into the BCD cavity, based on the energetic values reported in Table 2, leads us to the conclusion that, for this active principle, both complexes are stable and, since their difference in stabilization energy is small (3.35 kJ/mol = 0.80 kcal/mol), there is no preferential mode of insertion. Accordingly, at least under these conditions, the resulting situation should be a mixture of the two host–guest compounds. As in the case of Pipobroman, the largest stabilizing contribution is due to the dispersive van der Waals interactions (−91.04 kJ/mol for the Cl *OH prim* configuration, and −94.27 kJ/mol for the Cl *OH sec* configuration, respectively), although several, transients H-bonds are continuously formed and disrupted between the OH rims of the BCD and, alternatively, the carboxylic group and the nitrogen of the amino group of Melphalan, during the entire course of the simulation. Fig. 3(a) and (b) shows two snapshots of the molecular models of the two possible insertion modes of Melphalan after 400 ps of simulation, respectively. As we may see, in both configurations the Melphalan molecule has its central, hydrophobic core well immersed into the BCD cavity.

As concerns the H-bond pattern, a detailed analysis of the MD trajectory detects a stable interaction between the OH of the carboxyl group of the drug and a secondary BCD OH residue in the case of the Cl *OH prim* insertion, characterized by an average length of 1.8(±0.2) Å, whereas, in the Cl *OH sec* case, both the amino and the carboxyl group of Melphalan are, alternatively and non-permanently, involved in H-bonding with some primary BCD hydroxyl groups. These forces, coupled with the favorable value of the angle formed

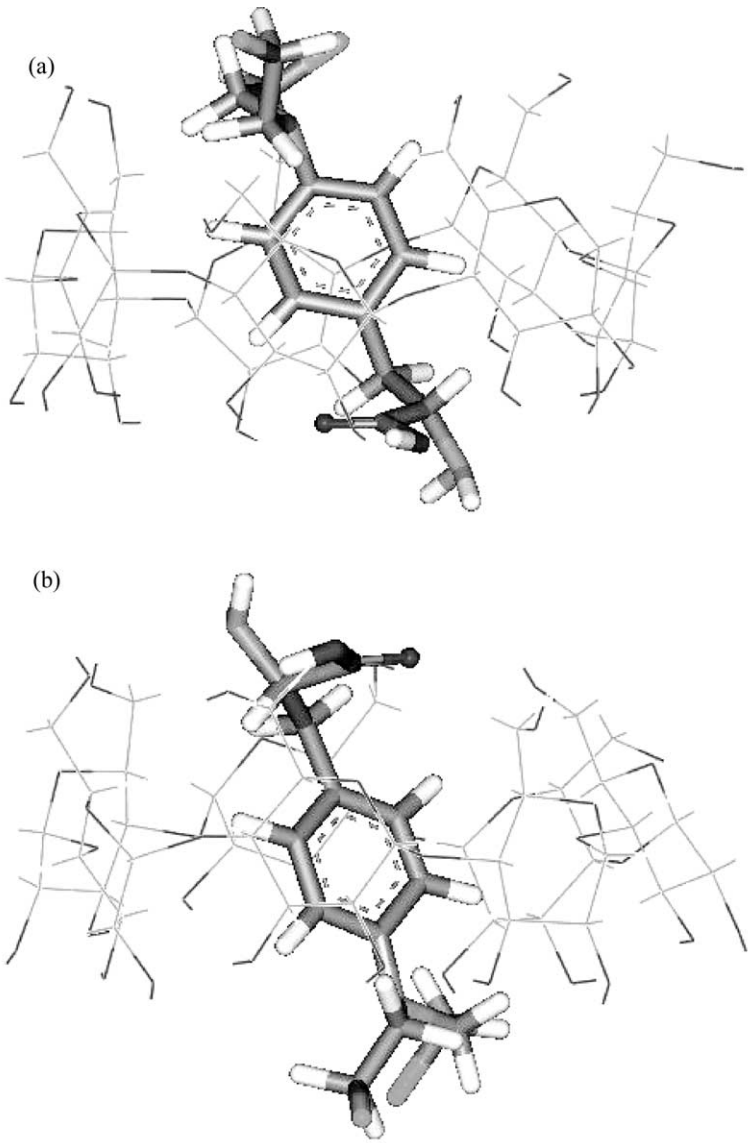

Fig. 3. Views of the equilibrium structures of the BCD–Melphalan complexes after 400 ps of MD simulation: (a) Cl *OH prim* configuration; (b) Cl *OH sec* configuration.

between the relative dipole moments of the drug and the BCD in both complexes (119° in the former case and 116° in the latter, see Table 3) account for the increased stabilization contribution from the Coulombic component of the potential energy (approximately 4.5 kJ/mol in both cases) with respect, for instance, to Pipobroman. Finally, contrarily to the case of Pipobroman, for the BCD–Melphalan inclusion complexes in both modes of insertion the valence contribution to the overall stabilization energy is positive, leading to an increase of approximately 6 kJ/mol, mainly ascribable to an increase in angle strain, necessary to best accommodate a bigger drug inside the BCD cavity.

An inspection of the values of tilt angle φ for both BCD–Melphalan host–guest compounds reveals that, again, the situation in both supermolecules is quite similar, both being characterized by a slight average inclination of the guest molecule with respect to the main BCD axis ($76 \pm 5°$ for the Cl *OH prim* and $75 \pm 6°$ for the Cl *OH sec*, respectively). The small average deviation of φ indicates that the aromatic ring of the Melphalan molecule is only slightly free to move inside the cavity, since the polar ends of the active drug remain fixed to the outer border by virtue of the constant presence of the H-bonds described above.

3.1.3. BCD–Acivicin

We now consider the results obtained for Acivicin, the most polar antitumor agents included in the present study ($\mu = 3.14$ D as obtained from the MD simulation on the isolated molecule). This relatively high polarity is bounded to its chemical structure, which consists of a chlorine-substituted isoxazole ring, further possessing the peculiar characteristic of an aminoacid. By virtue of its limited dimensions (calculated average molecular diameter = 5.19 Å, average molecular length = 4.48 Å), this drug should, in

principle, fit nicely into the BCD cavity, in both mode of insertion. Indeed, from an examination of the corresponding energetic values reported in Table 2 we can observe that the stabilization energies for Acivicin are favorable, and similar in value to those of Pipobroman. Also the contribution from the valence terms are rather small, being confined to 3.24 and 3.74 kJ/mol for the two inclusion complexes, respectively.

The difference of the stabilization energy between the Cl *OH prim* and the Cl *OH sec* configurations amounts to approximately 8 kJ/mol (~2 kcal/mol), so that, again, the resulting host–guest supermolecule should be, under these circumstances, a mixture of the two complexes. It must be observed that, also in this case, the small difference in the stabilization energy between the two possible configurations can be mainly ascribed to the van der Waals component of the non-bonded potential energy (−65.15 kJ/mol in the former and −77.36 kJ/mol in the latter situation). Fig. 4(a) and (b) shows two equilibrium configurations of the inclusion complexes of BCD and Acivicin corresponding to the two insertion modes after 400 ps of simulation, respectively.

An analysis of the entire trajectories of the simulations for the Cl *OH prim* complex indicates that there is a constant presence of alternative, fluctuating H-bonds for the entire period of the simulation which involve both the drug amino and carboxylic groups of Acivicin and some secondary OH residues of the carbohydrate macrocycle. The presence of these unstable and constantly evolving H-bonds allows for a greater degree of freedom of the drug inside the hydrophobic BCD cavity, as confirmed also by the analysis of the corresponding value of the tilt angle φ which, on average, is 14° out of the parallel alignment with the BCD axis but can fluctuate with time up to 26° around the equilibrium position. In the alternative orientation of the guest inside the host, we are faced with a different situation, since only one single but persistent H-bond of ADL = 2.6(±0.6) Å, between the drug carboxyl group and the OH residue of the BCD secondary rim, is present during the entire course of the MD simulation. This reflects both in a different orientation ($\varphi = 89°$ on average) and in a reduced mobility (±15°) of the drug inside the BCD hydrophobic domain.

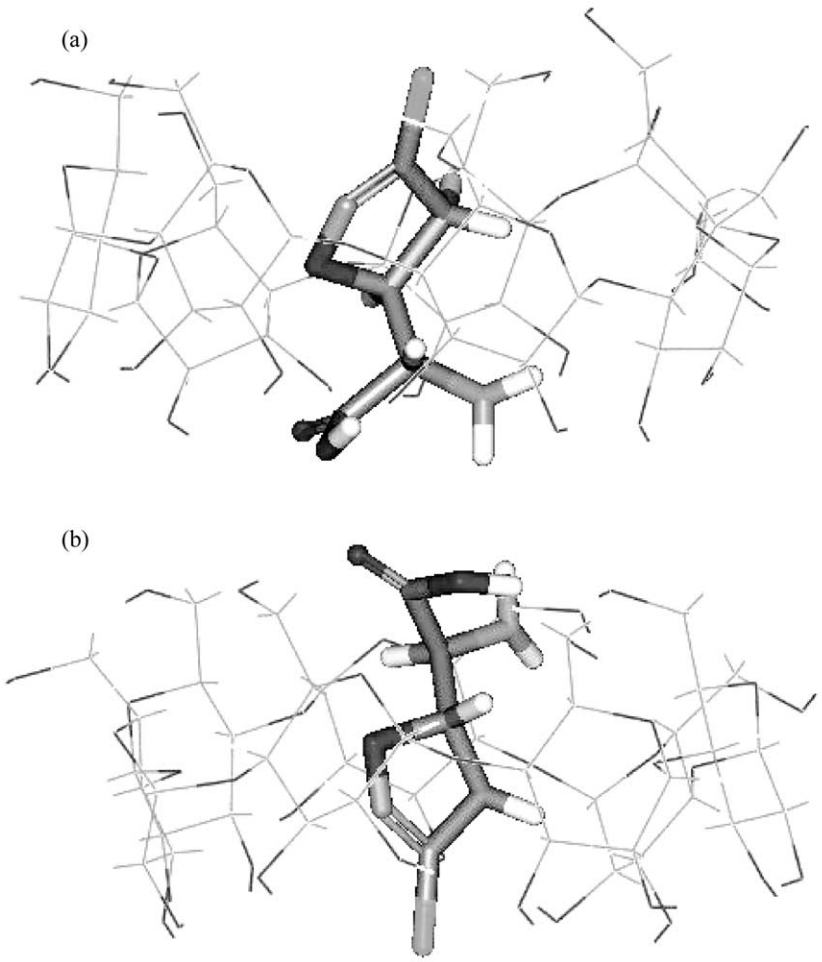

Fig. 4. Views of the equilibrium structure of the BCD–Acivicin complexes after 400 ps of MD simulation: (a) Cl *OH prim* configuration; (b) Cl *OH sec* configuration.

As could be expected, the electrostatic interactions are the most sensitive with respect to the orientation of the guest within the macrocycle. This is fairly evident if we consider the results concerning the dipole moments for both Acivicin–BCD complexes reported in Table 3. In the case of the complex Acivicin Cl *OH prim*, the dipole–dipole interaction is quite positive, as the two dipole vectors of the host and the guest are closer to the preferable antiparallel arrangement by forming an angle of 134°; on the contrary, for the alternative complex, the value of the corresponding

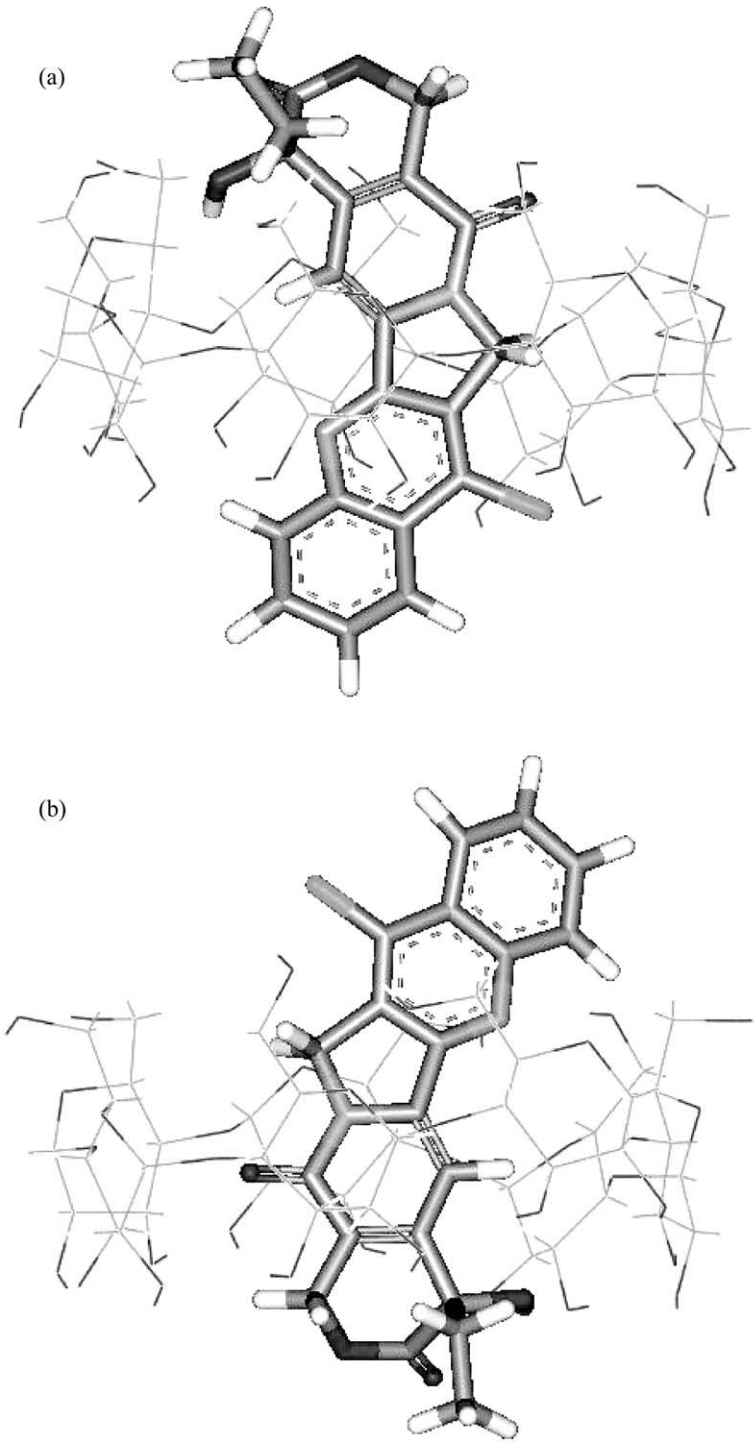

Fig. 5. Views of the equilibrium structure of the BCD–7-Chlorocamptotecin complexes after 400 ps of MD simulation: (a) Ethyl *OH prim* configuration; (b) Ethyl *OH sec* configuration.

angle is highly unfavorable (78° on average), thus resulting in an overall destabilization of 2.2 kJ/mol.

3.1.4. BCD–7-Chlorocamptotecin

The next drug considered is 7-Chlorocamptothecin. This drug, being a Camptothecin derivative, is characterized by quite big dimensions; nonetheless, by virtue of its long-narrow shape, it can possibly be inserted in the BCD cavity along the macrocyclic axis. As reported in Table 2, both inclusion complexes formed by this drug with the host molecule exhibit negative values of $(\Delta E_{1:1})_{NB}$; furthermore, these values are practically coincident. Accordingly, we can hypothesize that, under the conditions considered, the host–guest complexes can form and remain stable in a mixture of the two conformations. Fig. 5(a) and (b) shows two equilibrium configurations of the complexes of BCD and 7-Chlorocamptothecin, corresponding to the situation after 400 ps of molecular dynamics simulation. These snapshots reveal the considerable distortion the carbohydrate macrocycle must undergo in order to host the drug and to optimize their mutual interactions, which is quantified by the corresponding valence term contribution of 6.69 and 6.27 kJ/mol for the Ethyl *OH prim* and Ethyl *OH sec*, respectively.

The dipole–dipole interactions between the BCD and the present active principle are in complete agreement with the $(\Delta E_{1:1})_{NB}$ data. In fact, the energetically more stable conformation, Ethyl *OH sec*, presents a favorable arrangement of the BCD and drug dipoles, whose vectors form an average angle of 114°. On the contrary, the angle formed in the case of the complex Ethyl *OH prim* is less favorable, being equal to 96°.

In both complexes, the presence of a very limited number of unstable H-bonds due to the polar head jumps between different positions on the ring edges, do not appear to have any significant influence on the stability or on the magnitude of the tilt angle φ whose average values are 96°(± 16°) for the Ethyl *OH prim* configuration, and 77°(± 24°) for the opposite oriented complex, respectively. The difference in the mean values of these angles can be sensibly ascribed to the diverse position of the drug, considered with respect to the pyrrolidine ring, within the BCD cavity (see Fig. 5(a) and (b)).

3.1.5. BCD–Thiocolchicine

The next 1:1 complex analyzed concerns Thiocolchicine, an anticancer drug belonging to class 3. According to the characteristic dimensions of both the guest molecule and its host, only two parts of the active principle structure can be included in the BCD cavity: either the seven-member ring substituted with a methylthio group (5.93 Å average measured diameter), or the alternative, substituted phenyl ring (6.20 Å).

The simulation results lead to the conclusion that BCD can form stable complexes with Thiocolchicine by including the seven-member ring both in the S *OH prim* and S *OH sec* conformations. The change in total stabilization energy of the systems ranges from − 120.16 kJ/mol, for the S *OH prim* orientation, to − 110.63 kJ/mol for the S *OH sec* orientation (see Table 2). Whilst the dispersive component of the van der Waals forces have approximately the same magnitude, a different balance between the remaining energy components are displayed by these two different guest orientations. In particular, the electrostatic interaction slightly increases the energy of the system upon complexation in the former case (i.e. 0.46 kJ/mol), whereas for the latter the system is stabilized by 2.59 kJ/mol. As a further comment we can observe that, in the S *OH prim* complex, the most sterically hindered part of the drug molecule is placed in the proximity of the largest rim of the BCD, in order to minimize the repulsive van der Waals contacts between host and guest. A graphical illustration of this aspect is reported in Fig. 6(a) and (b), featuring four MD snapshots after 400 ps. As we clearly see, the seven term ring is better embedded in the BCD cavity throughout the entire simulation in the case of the S *OH prim* configuration. Nonetheless, an energy penalty equal to 11.31 kJ/mol for the S *OH prim*, and 13.84 kJ/mol for the *OH sec* insertion mode must be paid to adapt the host cavity to the size and shape of its guest.

As concerns the formation of stabilizing host–guest H-bonds, for the S *OH prim* complex the detailed analysis of the molecular trajectories reveals that several transient such intermolecular interaction takes place between the amide group of the drug and the OH groups of the narrower rim, thus contributing to the overall complex stability. On the other hand, the lack of persistent H-bonds in the S *OH sec* conformation allows for an enhanced mobility of the drug within the host cavity. The values of the tilt angle φ (79 ± 15° for the S *OH prim* complex, and 85 ± 21° for the S *OH sec* complex, respectively) are in agreement with the previous results.

Lastly, the angle values between the dipole vectors of the host and guest molecules indicate that, in both cases, no positive alignment is realized in either complex, as the vectors lay roughly perpendicular to one another (see Table 3), though the slightly greater value of 108° for the S *OH sec* assembly, coupled to a more favorable partial charge distribution within the complex components, may account for the lower value of $\Delta E_{1:1}^{coul}$ in this case.

3.1.6. BCD–Hexahydro-TMC69

The last drug considered is Hexahydro-TMC69. Similarly to 7-Chlorocamptothecin, this recently synthesized, potentially active anticancer principle is characterized by a long, narrow structure, with a peculiar L-shaped form. However, from the measurements of different molecular dimensions we can conclude that, in principle, neither its dimensions nor its shape can prevent its inclusion into the BCD.

Indeed, the results obtained from our simulations show that only a small variation in the valence energy is detected upon complexation in both cases (0.63 and 0.74 kJ/mol, respectively). Further, the values of $(\Delta E_{1:1})_{NB}$ for both situations are negative (see Table 2), implying that both complexes can be stable, the Octyl *OH prim* form being the most favored. Compared to all other drugs considered in this study, Hexahydro-TMC69 is the only one that exhibits a significant difference between the total non-bond energy components of the complexes formed ($\Delta(\Delta E_{1:1})_{NB}$·(Octyl *OH prim*–Octyl *OH sec* = −17.82 kJ/mol). Also, the alignment of dipole vectors (see Table 3), and the Coulombic energy, related to the charge distribution (see Table 2), contribute to enhance the stability of the Octyl *OH prim* complex.

Fig. 7(a) and (b) shows two equilibrium configurations—corresponding to the two possible insertions of Hexahydro-TMC69 into BCD—after 400 ps of dynamics simulation. The analysis of the entire molecular trajectories indicates that, in both complexes, there is a constant presence of some fluctuating H-bonds during the entire the period of the simulation. These bonds mainly

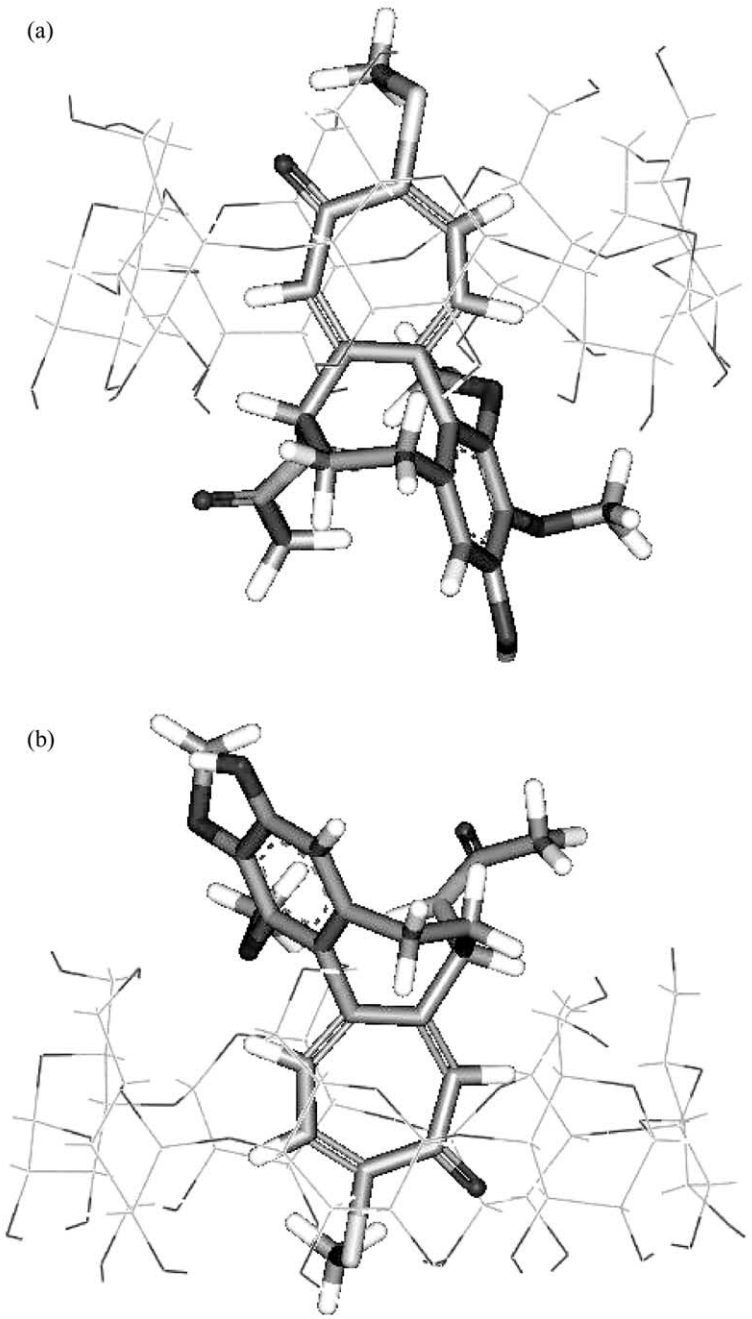

Fig. 6. Views of the equilibrium structure of the BCD–Thiocolchicine complexes after 400 ps of MD simulation: (a) S *OH prim* configuration; (b) S *OH sec* configuration.

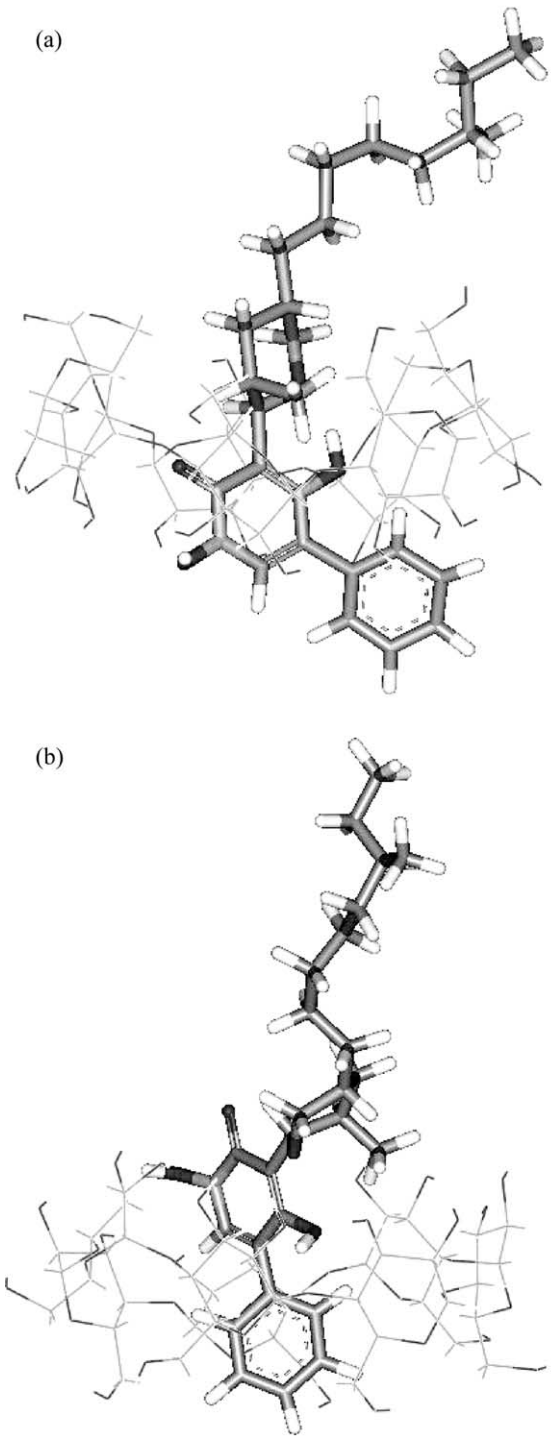

Fig. 7. Views of the equilibrium structure of the BCD–Hexahydro-TMC69 complexes after 400 ps of MD simulation: (a) Octyl *OH prim* configuration; (b) Octyl *OH sec* configuration.

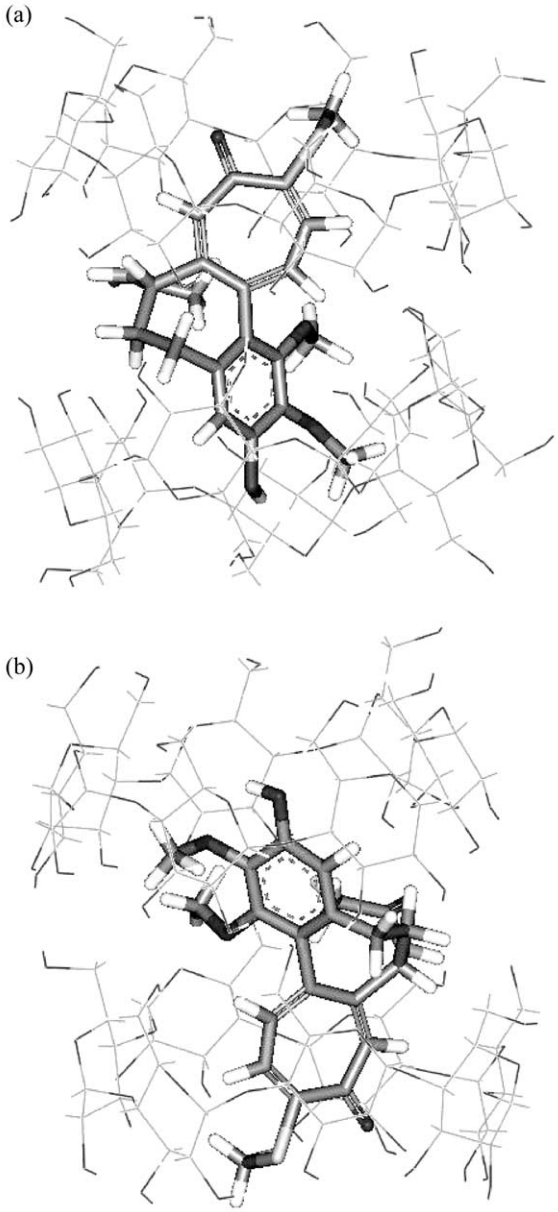

Fig. 8. Views of the equilibrium structure of the 2BCD–Thiocolchicine complexes after 400 ps of MD simulation: (a) *OH sec*/*OH sec* configuration; (b) *OH prim*/*OH sec* configuration.

involve the OH substituents of the heterocyclic ring of the drug and some secondary OH residues of the carbohydrate macrocycle. Notwithstanding the presence of these common intermolecular interactions, the drug assumes a somewhat different average orientation within its host cavity; accordingly, the values of the tilt angle φ and its range of variation are rather different for the two supermolecular species: $79 \pm 17°$ for Octyl *OH prim*, and $89 \pm 29°$ for Octyl *OH sec*, respectively.

3.2. 2:1 Complexation in the absence of explicit water solvent

According to the results discussed so far, all the host–guest complexes considered in a 1:1 stoichiometry have proven to be stable in the gas-phase equivalent conditions adopted for the simulation. Nevertheless, Figs. 6 and 7 clearly show how Thiocolchicine and Hexahydro-TMC69 can be only partially included within their host: in both

Table 4
Computed free drug energy, complexation energies $(\Delta E_{2:1})_{NB}$ and individual non-bonded complexation energy components obtained from MD calculations in the absence of explicit water solvent at 310 K for all the 2:1 complexes considered. All values are in kJ/mol

Guest	$(E_{drug})_{NB}$	$(\Delta E_{2:1})_{NB}$	$\Delta E^{d}_{2:1}$	$\Delta E^{r}_{2:1}$	$\Delta E^{coul}_{2:1}$
Thiocolchicine *OH prim–OH sec*	43.14	−160.33	−474.13	319.82	−6.02
Thiocolchicine *OH sec–OH sec*	43.14	−186.48	−454.55	266.06	2.01
6H-TMC69 *OH prim–OH sec*	81.13	−173.05	−368.99	201.67	−5.73
6H-TMC69 *OH sec–OH sec*	81.13	−163.64	−394.38	235.22	−4.48

All standard deviations (not reported for clarity) were of the order of one tenth of kJ/mol.

cases, in fact, a relevant part of the drug molecules remain outside the BCD cavity. From the vast literature concerning cyclodextrins, it is well known that these carbohydrate macrocycles may form complexes characterized by a 2:1 stoichioimetry as well. The question is naturally to be posed also about the energy gain upon association of a second guest molecule to the corresponding 1:1 complexes, i.e. the formation of 2:1 assemblies. Accordingly, for these two bigger compounds we decided to proceed and, starting from the lowest energy 1:1 complexes described above, we built and simulate the corresponding 2:1 host–guest systems. Again, we were faced with a problem of multiple configurations, since the second BCD ring can face the first either in the *OH prim*/*OH prim*, *OH prim*/*OH sec*, *OH sec*/*OH prim* or *OH sec*/*OH sec* configuration. However, after some preliminary, reasonable considerations based both on the stereochemical and the energetical features of the systems, we decided to consider only those 2:1 complexes in which the secondary rim (i.e. the largest one) of the additional BCD molecule was oriented toward the other BCD. Thus, the nomenclature of the resultant 2:1 complexes is characterized by denoting the type of the BCD rims that face each other in the inner part of the complex structure.

3.2.1. 2BCD–Thiocolchicine

Following the foregoing discussion, the 2:1 considered complexes of Thiocolchicine and BCD were the following: the *OH sec*/*OH sec*, deriving from the corresponding S *OH prim* 1:1 complex, and the *OH prim*/*OH sec* complex, originating from the S *OH sec* 1:1 assembly. Fig. 8(a) and (b) shows a snapshot of the complexes after 400 ps of simulation. If compared with the corresponding models of 1:1 stoichiometry (see Fig. 6), we can see that, in this case, the drug molecule is well surrounded by the two host cavities.

The energy components of all the 2:1 complexes analyzed are reported in Table 4. In the case of Thiocolchicine, both complexes exhibit highly negative values for $(\Delta E_{1:2})_{NB}$, indicating a good stability under the simulation conditions adopted. Of the two possible, alternative complexes, however, the energetic analysis seems to favor the *OH sec*/*OH sec* configuration by approximately 26 kJ/mol, which is a quantity large enough to conclude that, in the eventual mixture, this conformation should decidedly prevail over the other alternative. As expected, computations indicate that the drug molecule encounters less sterical hindrance n the *OH sec*/*OH sec* configuration, as the wider rim of the second BCD can easily adapt itself to accommodate a wide part of the molecule with respect to the primary OH network. Further, from a comparison of Tables 2 and 4 we can observe that both 2:1 complexes of Thiocolchicine with BCD present much lower energy values than the corresponding 1:1 forms. The stabilization energy gain between the S *OH sec* (1:1) and the *OH prim*/*OH sec* (2:1) complex is 49.72 kJ/mol, while the corresponding quantity between the S *OH prim* and the *OH sec*/*OH sec* is even greater, and equal to 66.32 kJ/mol, which leads us to conclude that, under these conditions and in excess of BCD, the complex between BCD and Thiocolchicine would primarily be characterized by a 2:1 stoichiometry.

In the case of the 2:1 host–guest assemblies, the dipole–dipole interactions are evaluated considering the dipole moment vector of the drug and the resultant dipole moment vector of the two BCDs. Accordingly, Table 5 lists the values of the corresponding angle formed by these two vectors. The alignments calculated for the Thiocolchicine 2:1 complexes are, in both cases, rather favorable, being equal to 129 and 114°, respectively. Finally, as concerns the relative orientation of the drug within the two cyclodextrin cavities, Thiocolchicine poses little problems since it presents a ring in the cavity of each of the two BCD molecules. Thus, it is possible to consider two different values for the tilt angle φ : the former, denoted φ_A, relative to the seven-member ring, and the latter, called φ_B, characterizing the substituted phenyl group. On average, the tilt angles of the *OH prim*/*OH sec* complex are equal to $\varphi_A = 92$ and $\varphi_B = 98°$, respectively, while those relative to

Table 5
Dipole moments μ (D) of the anticancer drugs in the 2:1 complexes, and average angle of interaction (deg) between the drugs and the BCDs in the 2:1 host–guest complexes obtained from MD simulations in the absence of explicit water solvent at 310 K

Anticancer drug	μ	$\text{Angle}_{\mu_{(host/guest)}}$
Thiocolchicine *prim–sec*	5.56	129
Thiocolchicine *sec–sec*	5.28	114
6H-TMC 69 *sec–sec*	2.55	83
6H-TMC 69 *prim–sec*	2.15	79

the alternative, *OH sec*/*OH sec* assembly, are $\varphi_A = 95°$ and $\varphi_B = 94°$, respectively. The analysis of the trajectories indicates that both complex structures are almost unaltered during the entire period of the simulations; for this reason, the systems appear to be rather stiff and the tilt angles reported above remain almost constant, being the standard deviation confined between 4 and 7°. This behavior strongly depends on the presence of a large number of H-bonds either—and to a lesser extent—between the drug and the cyclodextrin molecules, or between the two BCDs, thus creating a sort of capsular host–guest complex (Cram, 1988).

In conclusions, all evidences from our simulations let us speculate that, under the considered environmental conditions and in excess of BCD, this carbohydrate macrocycle and the antitumor drug Thicolchicine can originate a supermolecular assembly characterized by two host and one guest molecules, mainly oriented in the *OH sec*/*OH sec* configuration.

3.2.2. 2BCD–Hexahydro-TMC69

The last drug complexed with BCD in a 2:1 stoichiometry analyzed is Hexahydro-TMC69. In fact, the long aliphatic chain that protrudes from the BCD cavity in the corresponding 1:1 complexes seems suitable for inclusion in a second BCD molecule. Thus, according to the nomenclature explained above, the 2:1 considered complexes of Hexahydro-TMC69 are named *OH prim*/*OH sec* (i.e. the one deriving from the Octyl *OH prim* 1:1 complex) and *OH sec*/*OH sec* (i.e. the one deriving from the Octyl *OH sec* 1:1 conformation), respectively (see Fig. 9(a) and (b)).

As it could be anticipated, not only the total non-bond energy exhibit negative values for these complexes (see Table 4), but also, when compared to those of the corresponding 1:1 conformation, we observe a consistent increase in stabilization energy that equals approximately 59 kJ/mol in the case Octyl *OH sec* (1:1)–*OH sec*/*OH sec* (2:1), and 51 kJ/mol in the case Octyl *OH prim* (1:1)–*OH prim*/*OH sec* (2:1), respectively.

The values reported in Table 5 show that the dipole–dipole interactions are not particularly favorable—the dipole vectors lay almost perpendicular—even though the Coulomb energy term is negative, indicating an overall good charge distribution in the complexes. As regards the relative position and mobility of this drug within the macrocycle cavity, the presence of the second BCD molecule enveloping the long, aliphatic tails does not seem to influence much these two properties, being the tilt angle values very close to those measured in the case of the corresponding 1:1 conformation ($\varphi = 83 \pm 14°$ in for the *OH prim*/*OH sec*, and $\varphi = 82 \pm 17°$ for the *OH sec*/*OH sec*, respectively).

The analysis of the entire MD trajectories, in harmony with the preceding observations, reveals that both complexes tend to form only transients H-bonds between the drug and the macrocycles, and a less dense network of

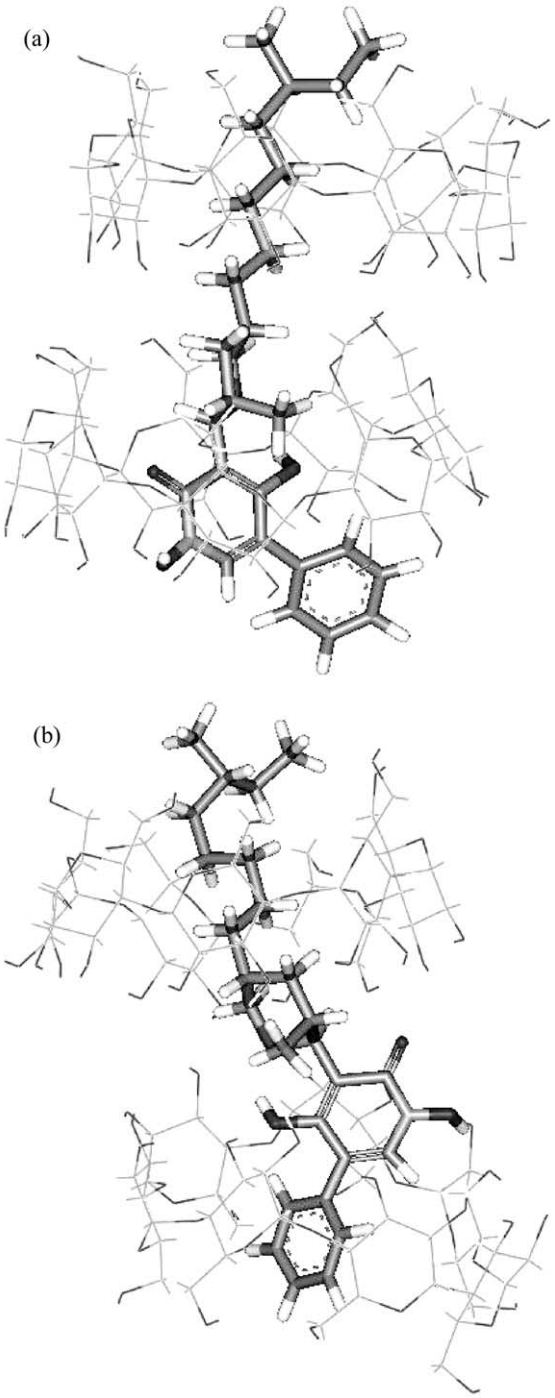

Fig. 9. Views of the equilibrium structure of the 2BCD–Hexahydro-TMC69 complexes after 400 ps of MD simulation: (a) *OH prim*/*OH sec* configuration; (b) *OH sec*/*OH sec* configuration.

the same intermolecular interactions between the two BCDs with respect to the case of Thiocolchicine. The latter aspect is a consequence of the relative positions of the two host molecules (Fig. 9): indeed, by virtue of the peculiar shape of the hosted drug, these are not aligned along their main axis, so only a limited part of the OH residues are in a suitable positions to mutually interact. Accordingly the structures

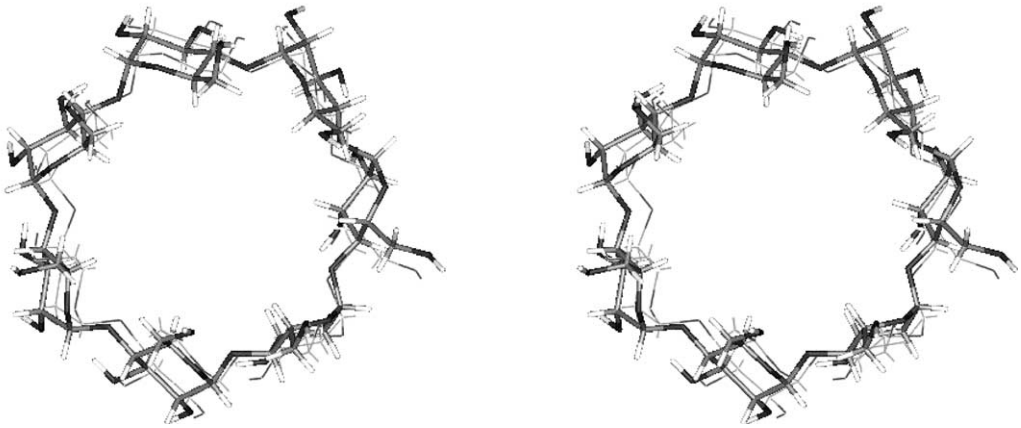

Fig. 10. Stereo view of the averaged crystal (thin) and solution structure (thick) of BCD.

appear also to be characterized by a grater mobility than those of the 2:1 forms of BCD–Thiocolchicine complex.

3.3. 1:1 Complexes in explicit water solvent

The experimental crystal structure and above described simulated model of BCD have a RMS deviation for all atoms of 0.15 and 0.10 Å for the non-hydrogen atoms only. These numbers imply that the differences between the time-averaged atomic positions obtained from the solution run and those obtained from the crystal run are significant only if they are larger than these values. The evidences from the water simulations reveal that the difference between the BCD conformation in solution and that in crystal is about four times larger: 0.54 Å averages over all atoms and 0.40 Å for the non-hydrogen atoms. Fig. 10 reports a comparison of the average crystal and solution structure of BCD.

A second observation is that, if we analyze the differences between the crystal and the solution conformation in terms of internal coordinated, we can say that the bond lengths, bond angles and glucose ring torsion angles do not show any significant difference in solution compared to the crystalline form, although the molecule is much more flexible in solution and can assume different shapes. Some exemplificative results are compared in Table 6, where the recommendations and symbols of nomenclature as proposed by IUPAC are followed (IUPAC-IUB Commission on Biochemical Nomenclature, 1970, 1971a,b). As we may see from Table 6, the torsion angles averaged over the solvated state dynamics are close to the corresponding X-ray crystal structure, and this can be considered a good result since neither crystal packing or symmetry was defined in the present study. Furthermore, all these values, including bond lengths and angles, are in excellent agreement with those obtained from a similar study by Momany and Willett (2000).

On the other hand, an analysis of the dynamics trajectories suggests that the O-6 atoms and the hydroxyl groups may attain positions in solutions that are significantly different from those in the crystalline state. Generally, these atoms show a larger mobility in solution, although some of them seem to constitute an exception, justified on the basis of a higher degree of hydrogen bonding in the solvated environment. In the simulation, the intramolecular hydrogen bonds are less stable in explicit water than in the presence of a continuum model for solvation, although the flip–flop character which has been observed both experimentally (Saenger, Betzel, Hingerty, & Brown, 1982) and by in vacuum simulation (Köhler, Saenger, & van Gunsteren, 1988; Mayer and Köhler, 1996) is still present. Further, hydrogen bonds that are

Table 6
Crystal structure and MD averaged (2.5 ns) structural parameters of BCD in water at 310 K. Distances are expressed in Å and angles in degrees

	Crystal	MD in water
O-4(n)–O-4($n-1$)	4.364,[a] 4.385[b]	4.45
O-2(n)–O-3($n-1$)	2.857,[a] 2.884[b]	2.89
C-1(n)–O-1(n)–C-1($n-1$)	117.7[a]	118.3
O-4(n)–O-4($n-1$)-O-4($n-2$)	128.3,[a] 128.3[b]	128.6
O-5(n)–C-1(n)–O-4($n-1$)–C-4($n-1$)	109.9,[a] 109.8[b]	110.6
O-4(n)–C-1(n)–O-4($n-1$)–C-1($n-1$)	168.9[a]	167.3
C-1(n)–O-4($n-1$)–C-4($n-1$)–C-3($n-1$)	128.3,[a] 127.6[b]	130.4
C-1(n)–O-4($n-1$)–C-4($n-1$)–O-4($n-1$)	−171.1[a]	−169.5

[a] Linder and Saenger (1982).
[b] Saenger et al. (1998).

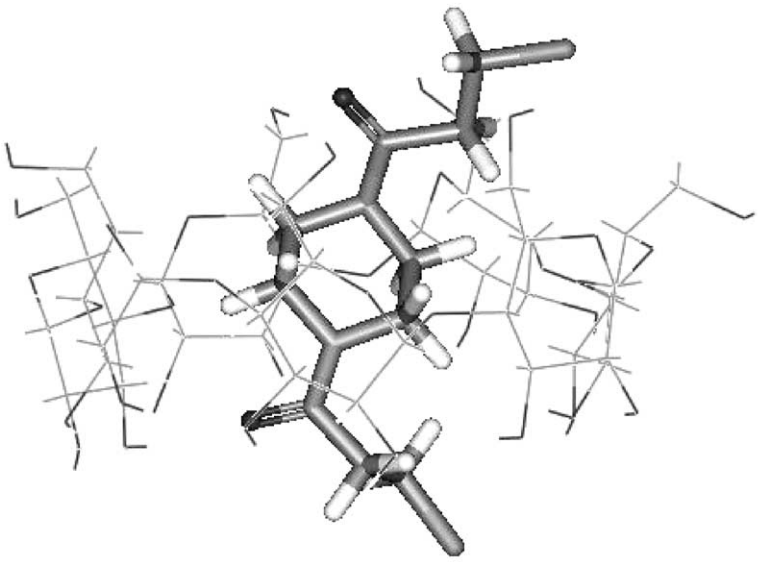

Fig. 11. View of the equilibrium structure of the BCD–Pipobroman complex after 2 ns ps of MD simulation.

present under the former conditions are observed in solution, but a number of H-bonds in solution are not observed for the isolated cyclodextrin. Accordingly, the structures observed and describe in the foregoing part of this study are only some members of a wide family of structures that are accessible to BCD in solution as, in aqueous solution, the molecule clearly visits a larger part of the conformational space than it does in continuum solvation model simulation.

3.3.1. BCD–Pipobroman

The first host–guest inclusion complex considered was BCD–Pipobroman. Fig. 11 reports, as an example, a model of the equilibrium structure of this complex after 2 ns simulation time. It shows that the drug has the piperazinic ring well set at the center of the BCD cavity, while dynamic H-bonds continually form and disrupt either between water and BCD, or between water and the polar ends of the active principle. Another noteworthy feature of this dynamic study

Table 7
Energy terms and total binding free energy for BCD complexed with the six anticancer drugs considered at 310 K. All values are in kJ/mol

Contribution	Pipobroman	Melphalan Cl *OH prim*	Melphalan Cl *OH sec*	7-Chloro-Camptotecin Ethyl *OH prim*	7-Chloro-Camptotecin Ethyl *OH sec*
ΔG_{int}^{ele}	−87.32 ± 1.10	−95.52 ± 1.31	−96.27 ± 1.55	−131.46 ± 2.00	−134.92 ± 2.32
ΔG_{int}^{vdW}	−107.57 ± 1.80	−108.11 ± 1.00	−103.23 ± 1.22	−100.13 ± 1.57	−104.92 ± 1.92
ΔG_{int}^{val}	5.87 ± 0.11	16.32 ± 0.45	14.65 ± 0.62	7.25 ± 0.88	7.38 ± 0.96
ΔG_{MM}	−189.02 ± 2.79	−187.31 ± 1.86	−184.85 ± 2.15	−224.34 ± 2.69	−232.46 ± 3.28
ΔG_{sol}^{np}	−9.63 ± 0.04	−10.24 ± 0.05	−10.24 ± 0.05	−10.83 ± 0.08	−10.83 ± 0.08
ΔG_{sol}^{ele}	188.88 ± 1.41	185.00 ± 1.80	184.61 ± 1.85	222.99 ± 1.45	230.88 ± 1.66
ΔG_{sol}	179.25 ± 1.37	174.76 ± 1.75	174.37 ± 1.80	212.16 ± 1.37	220.05 ± 1.58
ΔG_{tot}^{ele}	91.93 ± 0.27	79.24 ± 0.44	78.10 ± 0.25	80.7 ± 0.63	85.13 ± 0.74
$T\Delta S$	10.17	5.88	5.74	5.41	5.64
ΔG_{bind}	−19.94	−18.43	−16.22	−17.59	−18.05
Contribution	Thiocolchicine S *OH prim*	Thiocolchicine S *OH sec*	6H-TMC 69 Octyl *OH prim*	6H-TMC 69 Octyl *OH sec*	
ΔG_{int}^{ele}	−84.13 ± 1.11	−75.47 ± 0.91	−82.47 ± 1.31	−82.53 ± 1.33	
ΔG_{int}^{vdW}	−56.85 ± 0.68	−42.64 ± 0.51	−47.86 ± 1.00	−47.91 ± 1.01	
ΔG_{int}^{val}	11.18 ± 0.84	17.42 ± 0.95	21.10 ± 0.98	21.53 ± 0.99	
ΔG_{MM}	−129.80 ± 0.95	−100.69 ± 0.47	−109.23 ± 1.33	−108.91 ± 1.35	
ΔG_{sol}^{np}	−11.59 ± 0.11	−11.59 ± 0.11	−13.24 ± 0.10	−13.24 ± 0.10	
ΔG_{sol}^{ele}	138.92 ± 0.87	116.84 ± 0.62	110.74 ± 2.05	110.43 ± 2.09	
ΔG_{sol}	127.33 ± 0.76	105.25 ± 0.51	97.50 ± 1.95	97.19 ± 1.99	
ΔG_{tot}^{ele}	43.20 ± 0.53	29.78 ± 0.40	15.03 ± 0.64	14.66 ± 0.57	
$T\Delta S$	10.17	9.46	4.87	4.92	
ΔG_{bind}	−12.64	−4.90	−16.60	−16.64	

is that no water molecules were found inside the BCD cavity, because the guest displaced the water molecules present inside. However, two water molecules have been observed to lie close to the bottom of the cavity, in the proximity of the secondary rim and in position suitable for hydrogen bonding with the OH groups of BCD.

Interestingly, the value of the tilt angle φ is very close to 90° (i.e. 95 ± 9°). If compared with the results described previously, we can see that the interactions with water molecules further reduce the free of movement of the drug inside the cavity and contribute to maintain it almost parallel to the BCD axis.

The estimated free energy of binding ΔG_{bind} for this molecular assembly, obtained from the procedure detailed in Section 2, is reported in Table 7. In the complex, there is a decrease in free energy, as expected, due to the favorable enthalpy term ($\Delta H = \Delta G_{\text{MM}} + \Delta G_{\text{sol}} = -9.77$ kJ/mol). A negative enthalpy change can be associated to the release of energy from the system upon binding, accompanying dipole and van der Waals interactions. In addition, this loss of heat on complexation could correspond to the energy released on the expulsion of the enthalpy rich water molecules from the cyclodextrin cavity and from the guest's hydration sphere, and the subsequent establishment of the non-bonding host–guest intermolecular forces (Griffiths and Bender, 1973; Menard, Dedhiga, & Rhodes, 1990; Tabushi, Kiyosuke, Sugimoto, & Yamamura, 1978). As concerns the electrostatic contribution to ΔG_{bind}, it is very important to consider the electrostatic component of the molecular mechanics energy $\Delta G_{\text{int}}^{\text{ele}}$ together with the electrostatic contribution to solvation $\Delta G_{\text{sol}}^{\text{ele}}$ when examining the role of electrostatics in any host–guest complex formation. In fact, as proven by several studies (Bruccoleri, Novotny, & Davis, 1997; Misra, Sharp, Friedman, & Honig, 1994; Novotny, Bruccoleri, Davis, & Sharp, 1997; Novotny & Sharp, 1992; Sharp, 1996; Shen & Wendoloski, 1996), electrostatics generally disfavor the docking of a ligand/receptor couple because the unfavorable change in the electrostatic of solvation is mostly, but not fully, compensated by the favorable electrostatics within the resulting host–guest complex. Indeed, the total electrostatic energy contribution $\Delta G_{\text{tot}}^{\text{ele}}$ to the binding free energy for the BCD/Pipobroman complex is not favorable, with value of 91.93 kJ/mol. Thus, even though electrostatics tends to destabilize the complex formation, it is the optimized balance of opposing electrostatic contributions and a more favorable dispersion term that leads to the drug binding by BCD.

We also see from Table 7 that the sign of apparent entropy ΔS is positive, and equal to 32.8 J/mol K. Rather generally, guest inclusion is associated with an entropy decrease; on the other hand, removal of the water molecules from the cavity and from the hydration sphere of the guest is also associated with an entropy increase, typical of hydrophobic binding. The hydrophobic (solvent entropy) effect, which drives the association of non-polar surfaces of molecules by excluding water molecules from the interface, is believed to contribute to ΔS (Jelesarov, Leder, & Bosshard, 1996; Murphy, Freire, & Paterson, 1995; Raman, Allen, & Nall, 1995; Schwarz, Tello, Goldbaum, Mariuzza, & Poljak, 1995; Torigoe et al., 1995; Tsumoto et al., 1996; Zidovetzki, Blatt, Schepers, & Pecth, 1988). Indeed, the entropic gain due to solvent release from the binding site seems to be a common feature of biological systems by which they overcome the energy cost if creating apparent order out of chaos.

Enthalphy/entropy compensation is a term utilized to describe the behavior of ΔH and ΔS for a series of similar reactions driven by changes in solvation (Lumry & Rajender, 1970), and is observed in the vast majority of cyclodextrin complexes, the phenomenon stemming from a common inclusion mechanism of binding, irrespective of the guest (Clarke, Coates, & Lincoln, 1988). This compensatory behavior is considered to be extra-thermodynamic, and not an obvious consequence of thermodynamic law. Hydrophobic forces associated with the change in solvation of each molecule are thought to be responsible for the compensation effect observed in aqueous systems. To try quantifying the hydrophobic interaction contribution to the solvation energy in the binding process of anticancer drugs to BCD, we have adapted the approach proposed by Raschke, Tsai, and Levitt (2001), according to which such component of the free energy is proportional to the loss in exposed molecular surface area (ESA). Due to the fact that the interior of the cavity of BCD is hydrophobic, and that the cavity volume is confined, the calculation of ESA, estimated using the modified version of the Connolly algorithm (Fermeglia & Pricl, 1999), was performed only over the hydrophobic atoms of each guest molecules which are inserted in the BCD cavity, and with a probe radius equal to 1.4 Å.

In the case of Pipobroman, this calculation yields a value for the contribution of hydrophobic interaction to binding free energy of 34.31 kJ/mol, and this value seems to confirm the hypothesis that, for this given assembly, simple van der Waals interactions and atomic point-charge electrostatics account for the most important driving force in biocompatibility.

Finally, we can remark here that the value of ΔG_{bind} for the BCD/Pipobroman complex, corresponding to an apparent stability constant for the first order complex $K_{1:1}$ calculated association constant of $3.128 \times 10^3\ M^{-1}$, is in excellent agreement with the corresponding experimental values for a wide variety of BCD-drug inclusion compounds characterized by a 1:1 stoichiometry (for a variety (by no means exhaustive) of different drugs in BCD see, for instance: Botsi, Yannakopoulou, Hadjoudis, & Waite, 1996; Dordunoo & Burt, 1996; Fujisawa, Kimura, & Takagi, 1997; Irwin et al., 1999; Ma, Rajewski, & Stella, 1999; Másson, Loftsson, Jónsdóttir, Fridriksdóttir, & Petersen, 1998; Mura et al., 1998; Nesnas, Lou, & Breslow, 2000; Oh, Lee, Lee, Shin, & Park, 1998; Rekharsky & Inoue, 1998; Valero, Costa,

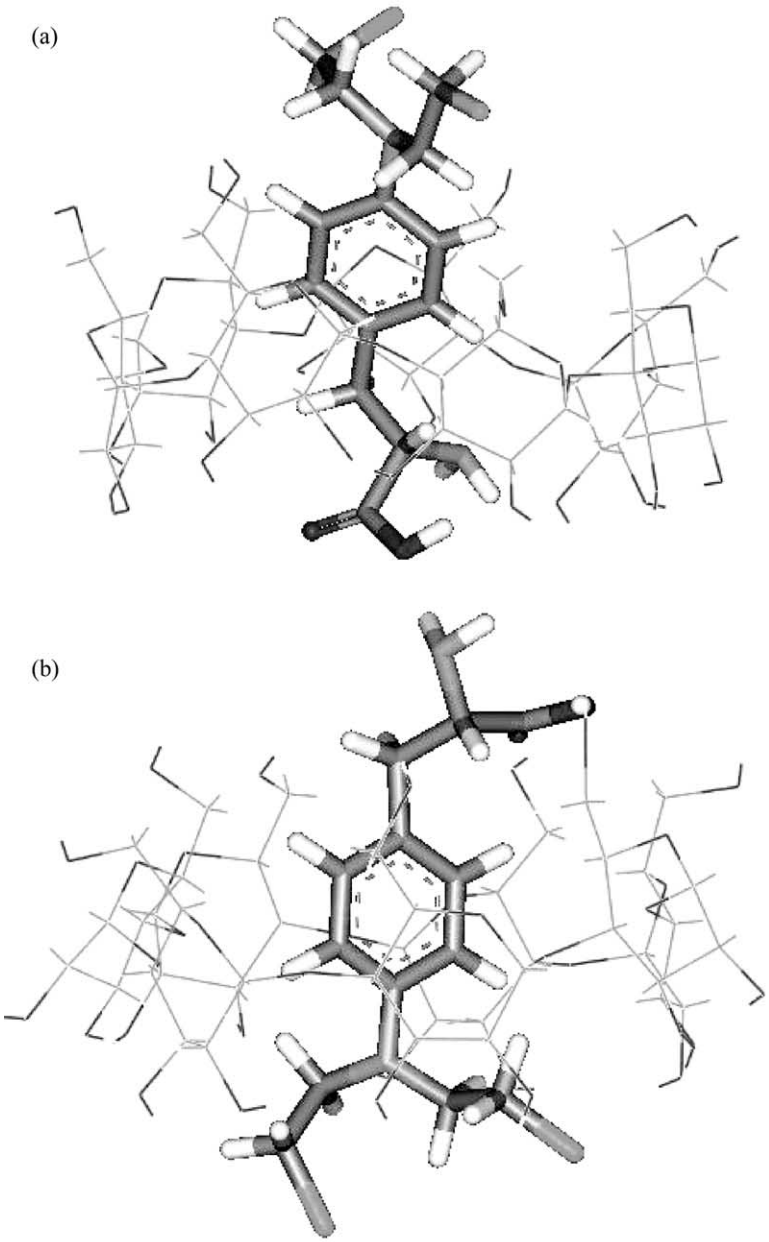

Fig. 12. Views of the equilibrium structures of the BCD–Melphalan complexes after 2 ns of MD simulation: (a) Cl *OH prim* configuration; (b) Cl *OH sec* configuration. Water molecules have been removed for clarity.

Ascenso, Velázquez, & Rodríguez, 1999; Velasco, Carmona, Muñoz, Guardado, & Balón, 1999; Yang & Breslow, 1997; Yuan, Zhu, & Han, 1999).

3.3.2. BCD–Melphalan

The second drug considered is Melphalan. Fig. 12(a) and (b) shows two snapshots of the molecular models of the two possible insertion modes of Melphalan after 2 ns of simulation. In both cases, the phenyl ring of the drug is well inserted into the BCD cavity, where the presence of two water molecules (not shown in the figures), together with other two at the mouth of the cavity between the aminoacid group and the BCD, is also observed for the entire period of the simulation. This fact has already been detected, particularly in the insertion of aminoacids and small peptides in BCD, and has been hypothesized to exert a favorable contribution to the complex stabilization (Miertuš et al., 1999b). Indeed, several H-bonds between the amino and carboxylic groups of the drug and the BCD OH residues are detected during the MD run, which however break down and reform, due to the formation of intermolecular H-bridges with the neighboring water molecules and to the exchange of the corresponding donor and acceptor. In particular, the slight average inclination of the guest molecule with respect to the main BCD axis in the case of the Cl *OH prim* configuration ($98 \pm 9^{\circ}$) indicates that

the aromatic ring of the Melphalan molecule is only slightly free to move inside the cavity, since the polar ends of the active drug remain fixed to the outer border by virtue of the constant presence of the H-bonds described above. On the other hand, in the opposite mode of insertion the analysis of the corresponding value of the tilt angle φ reveals that, on average, this quantity is 17° out of the parallel alignment with the BCD axis, and can fluctuate with time up to 12° around the equilibrium position. This is in agreement with the smaller density of H-bonding detected during the MD run when the aminoacidic group protrudes from the OH primary rim.

Table 7 lists the calculated free energy of binding and the relative components for both Melphalan insertions in BCD; again, the values of ΔG_{bind} gathered from the simulations are in the range of the experimentally derived values for a set of similar compounds. Our estimates reveal that the energy balance favors the Cl *OH prim* insertion mode. For both configurations, the effective formation of the complexes is driven by the molecular mechanics interaction energy components and the non-polar contribution to solvation; further, these energetic terms are similar for both orientations. The total electrostatic contributions for both complex formations are again unfavorable, being equal to approximately 79 and 78 kJ/mol, but the net energetic result is favored by the positive balance between opposing electrostatic terms.

In a recent study, Liu, Li, and Guo (2000) formulated a non-linear free energy model for the inclusion complexation of cyclodextrin with 1,4-disubstituted benzenes (X–C_6H_4–Y) in aqueous solutions. According to the model, the microscopic binding constant for a specific complexation orientation, for example, the orientation in which the X group points towards the primary OH rim, obeys the following equation:

$$\ln K_X = 0.166R_X + 0.139\pi_X + 1.44\sigma_X - 1.27\sigma_Y + 2.51 \quad (7)$$

in which the substituent molar refraction R, hydrophobic constant π and Hammett constant σ reflect van der Waals forces, hydrophobic interactions and electronic effects in the inclusion complexation, respectively.

Similarly, the microscopic binding constant for the opposite orientation, in which the Y group points towards the primary hydroxyls of BCD, is given by the following relationship:

$$\ln K_Y = 0.166R_Y + 0.139\pi_Y + 1.44\sigma_Y - 1.27\sigma_X + 2.51 \quad (8)$$

Calculations using the above equations and the parameters of the substituents given by Wu (1997), indicate that, for the BCD/Melphalan complex in the orientation Cl *OH prim*, the corresponding $K_{1:1}$ (1394 M^{-1}) is significantly larger than the binding constant for the opposite orientation, Cl *OH sec* (467 M^{-1}). Since the Hammett σ constants for the two substituents of Melphalan are almost coincident (−0.36 for the CH_2–CH(COOH)NH_2 group, and −0.37 for the $N(CH_2Cl)_2$ group), these results confirm that the dispersion forces and hydrophobic interactions, coupled with solvation contribution, are most likely responsible for such a result.

Somewhat serendipitously, the values of ΔG_{bind} obtained from the above 1:1 stability constants (18.66 and 15.84 kJ/mol for the Cl *OH prim* and the Cl *OH sec* configuration, respectively), are very close to those we determined by molecular simulations (see Table 2). Further, the range of the values obtained are in good agreement with those evaluated experimentally by Ma et al. (1999), for the inclusion of Melphalan in $(SBE)_{7m}$-BCD and HP-BCD.

Finally, the calculation of the hydrophobic contribution to binding yields a value of 34.49 kJ/mol, in reasonable agreement with the corresponding value found for Pipobroman.

3.3.3. BCD–Acivicin

We now consider the results obtained for Acivicin. The inspection of the molecular trajectories of the BCD/Acivicin complexes deriving from the two possible insertion modes (Cl *OH prim* and Cl *OH sec*, respectively) reveals a behavior which differs from all other anticancer active principles considered; indeed, both complexes were found to be unstable in water, and, after 1 ns, the Acivicin molecules was found outside the BCD cavity. Fig. 13(a) and (b) shows this fact. In a way, this could be considered an expected result. In fact, for single, small and polar aminoacids, solvation free energy calculations have shown that these guest molecules will be more stabilized in water, thus preventing the formation of an inclusion complex in BCD (Miertuš et al., 1999a,b). To support this observation, we report here the corresponding value of the solvation Gibbs free energy ΔG_{sol} obtained from the simulation of the isolated drug molecule, which is largely negative and equal to −138.00 kJ/mol. This suggests the occurrence of strong interactions of Acivicin with bulk water, and justifies the larger preference of this drug (characterized by a dipole moment of 4.9 D in water, as obtained from the MD simulations) for the solvent rather than for the formation of the BCD inclusion complexes.

Although apparently in contrast with our previous finding (see Section 3.1.3), where both complex configurations appeared to be stable in the smaller time interval considered (500 ps), these results are not entirely surprising since, despite the small dimensions of Acivicin, the stabilization energy values calculated without explicit waters were the lowest obtained for the entire set of drug analyzed, and this was already justified on the basis of the high polar character of this active principle.

3.3.4. BCD–7-Chlorocamptotecin

Fig. 14(a) and (b) shows two equilibrated structures, corresponding to the two alternative orientations of 7-Chlorocamptotecin within the BCD cavity, after 2 ns of MD. The analysis of both entire molecular trajectories reveals that the drug is fairly limited in its movement within its host, and is always well inserted into the BCD cavity,

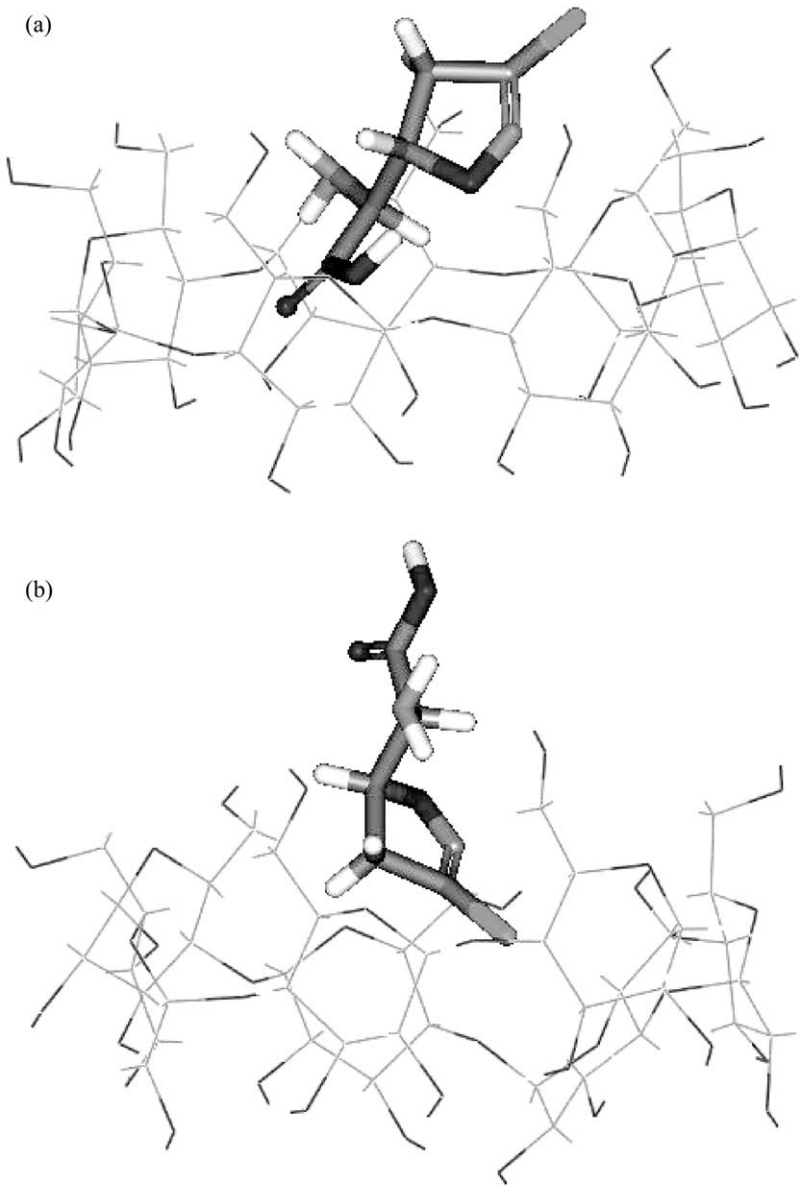

Fig. 13. Views of the equilibrium structures of the BCD–Acivicin complexes after 1 ns of MD simulation: (a) Cl *OH prim* configuration; (b) Cl *OH sec* configuration. Water molecules have been removed for clarity.

where also three water molecules are trapped at the proximity of the BCD mouth. In both complexes, the presence of a very limited number of unstable intermolecular H-bonds, due to the polar head jumps between different positions on the ring edges, do not appear to have any significant influence neither on the stability nor on the magnitude of the tilt angle φ, whose average values are 117°(±6°) for the Ethyl *OH prim* configuration, and 74°(±6°) for the opposite oriented complex, respectively.

Interestingly enough, the results of the energy terms and the binding free energy for the BCD complexed with 7-Chlorocamptotecin reported in Table 7 indicates similar values for ΔG_{bind} for both inclusion modes, in agreement with the preceding experiments. Evidently, the largest input to the binding energy for these complexes comes from the gain in van der Waals and hydrophobic interactions, which is not canceled out by unfavorable changes in solvation free energies. Again, the calculated entropy variation is positive, although somewhat smaller than in the previous case since, as discussed above, some solvent molecules remain structured within the BCD cavity. The corresponding contribution of hydrophobic forces to binding is estimated to be 31.51 kJ/mol.

Finally, to testify the reliability of the predicted values for ΔG_{bind} for this complexes we can observe that, for a series of heteroanthracene rings modified by the presence of polar groups (Yuan, Zhu & Han, 1999), and mainly for Resorcinol Blue, whose shape and calculated molecular

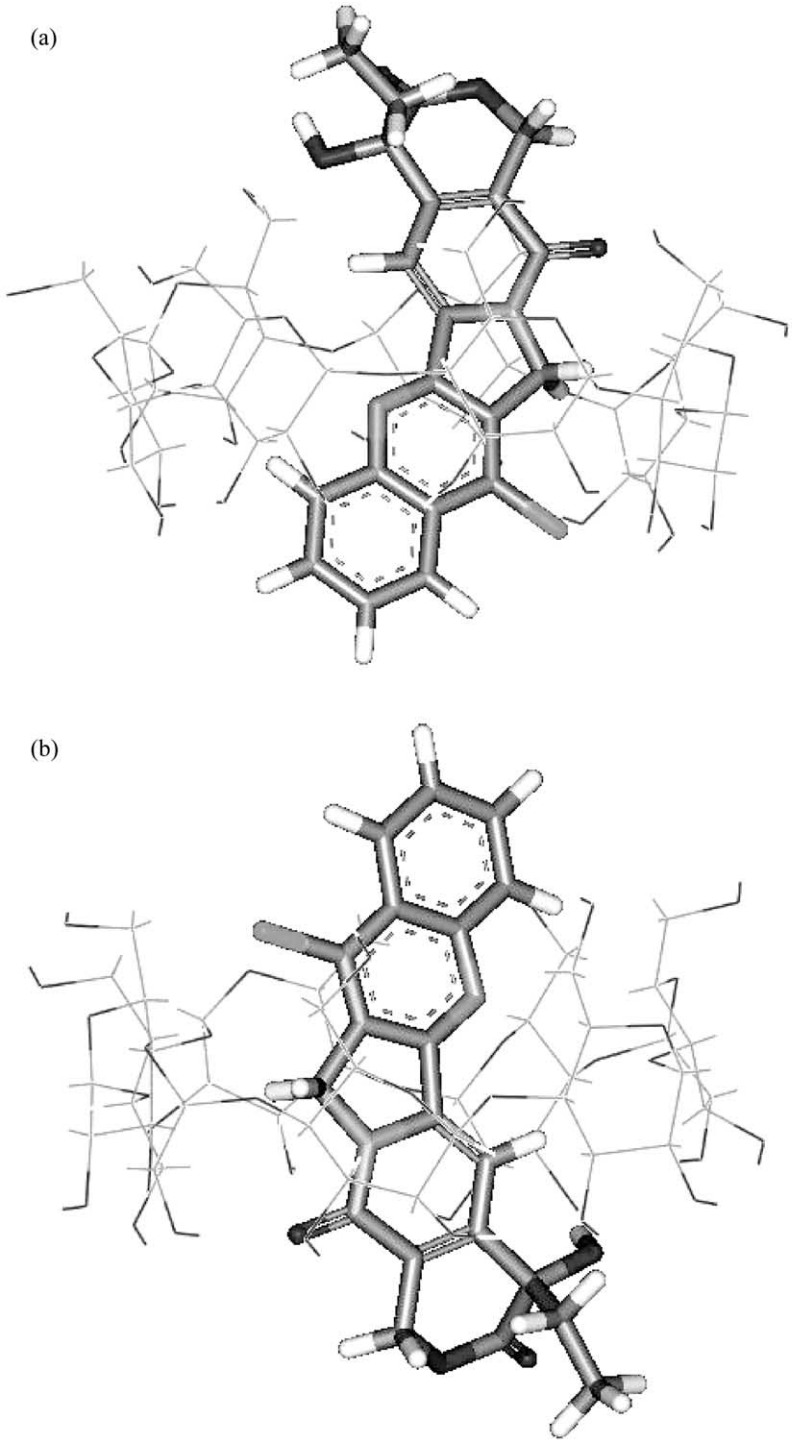

Fig. 14. Views of the equilibrium structures of the BCD–7-Chlorocamptotecin complexes after 2 ns of MD simulation: (a) Ethyl *OH prim* configuration; (b) Ethyl *OH sec* configuration. Water molecules have been removed for clarity.

surface area are similar to those of 7-Chlorocamptotecin, the experimentally determined range of $K_{1:1}$ values are in good agreements with our findings.

3.3.5. BCD–Thiocolchicine

Our experiments in the absence of water molecules have shown that this drug can form stable inclusion complexes with BCD, in which the seven-member ring carrying the SCH_3 moiety is inserted in the host cavity. Accordingly, we investigated the behavior of the corresponding complexes within the water solvent. Fig. 15(a) and (b) shows two snapshots corresponding to the two different orientation of the drug into the BCD (S *OH prim* and S *OH sec*, respectively), after 2 ns of MD. It can be observed that, in

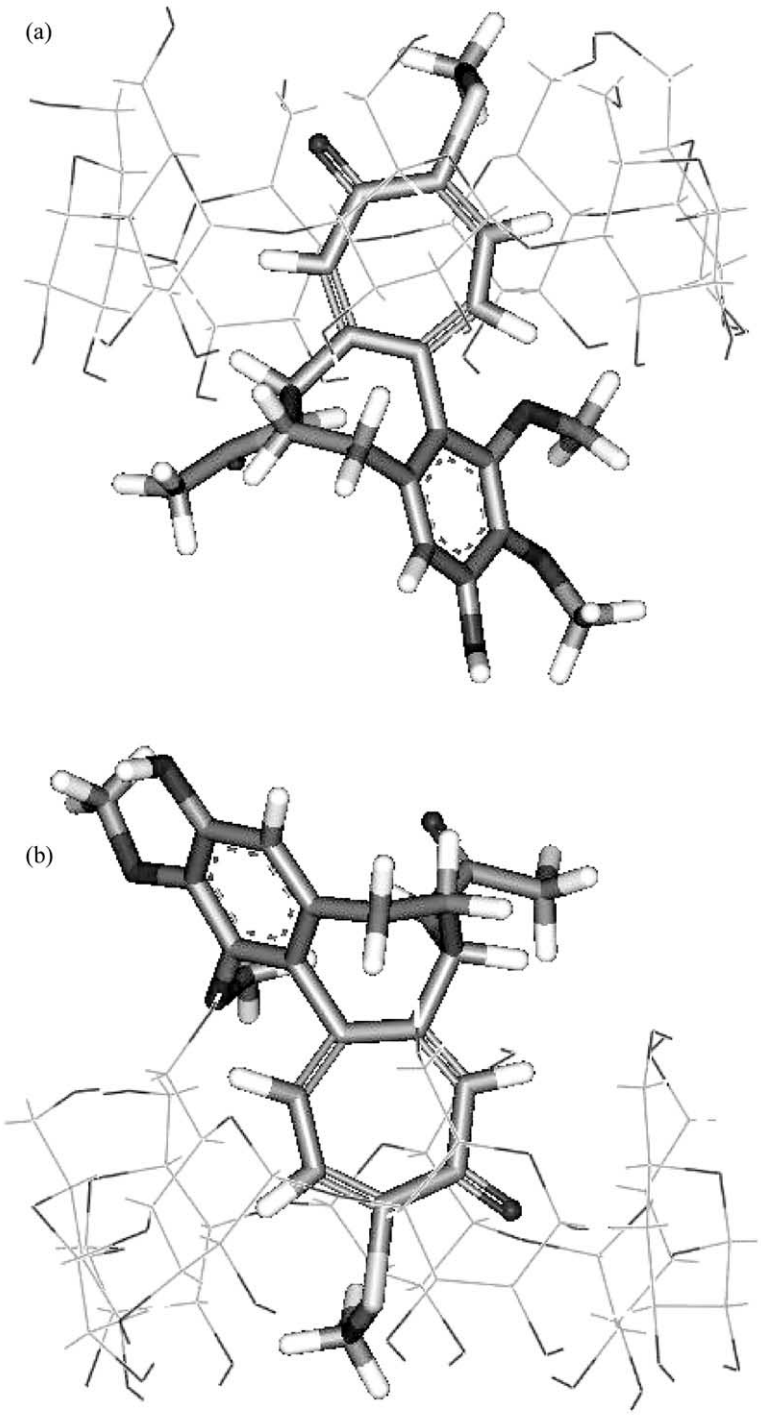

Fig. 15. Views of the equilibrium structures of the BCD–Thiocolchicine complexes after 2 ns of MD simulation: (a) S *OH prim* configuration; (b) S *OH sec* configuration. Water molecules have been removed for clarity.

the S *OH prim* configuration, the seven-member ring is better included in the cavity with respect to the opposite situation, and this evidence persists during the entire period of simulation.

The presence of some unstable H-bonds has a negligible influence on the stability of both the configurations, but allows for a freedom of movement of the drug within its host. The S *OH prim* equilibrium configuration has no water molecules trapped in the BCD cavity, and presents an average tilt angle φ equal to $73^\circ(\pm 19^\circ)$; on the contrary, in the S *OH sec* complex the ring is less well inserted in the cavity ($61 \pm 26^\circ$), where also the constant presence of two water molecules at the edge of the carbohydrate macrocycle can be detected.

In agreement with the previous experiments, the values of ΔG_{bind} reported in Table 7 seem to favor the S *OH prim* inclusion mode, being the corresponding calculated values of the binding constants $K_{1:1}$ equal to 164.31 M^{-1} for the S *OH prim*, and 7.32 M^{-1} for the S *OH sec*, respectively. It is worthwhile noticing here that the former value of $K_{1:1}$ is in good agreement with those found for the complexation of a drug of close structure and dimensions such as diazepam in different CD derivatives (Másson et al., 1998).

A different balance between the energy components are displayed in the values of ΔH of the two complex configurations (−2.47 kJ/mol for the S *OH prim* and 4.56 kJ/mol for S *OH sec*, respectively). Although the cavity solvation contribution is accompanied by a lower increase of energy in the S *OH sec* case, this is not parallel by the stabilization due to the molecular mechanics energy components, which lead to a stronger decrease in energy that favors the S *OH prim* orientation by about 30 kJ/mol.

As already seen for the other complexes, the calculated entropy variation has a positive and rather high value in both cases. Furthermore, we can speculate that the slightly smaller number for the S *OH sec* complex possibly relates to the presence of some solvent molecules within the BCD cavity. The value of the contribution of hydrophobic forces to binding (which can be calculated in 31.93 kJ/mol) reflects the fact that, despite the drug dimensions, the number of non-polar atoms actively contributing to these interactions are almost the same as in the previous cases.

3.3.6. BCD–Hexahydro-TMC69

The last drug considered is Hexahydro-TMC 69. Fig. 16(a) and (b) shows the conformations, after 2 ns of MD, corresponding to the two different orientations of the drug, Octyl *OH prim* and Octyl *OH sec*, respectively. They show that the drug remains very well inserted in the BCD cavity, originating an assembly that closely resembles the corresponding isolated supramolecular structures.

The analysis of the entire trajectories of the MD simulations indicates that, for both complexes, only some unstable H-bonds are formed in both cases. Moreover, the presence of one trapped water molecule inside the BCD cavity in the Octyl *OH sec* equilibrium conformation is evidenced. These aspects account for the different average values of the tilt angle φ and its variation: 71 ± 20° for Octyl *OH prim* and 94 ± 12° for Octyl *OH sec*, respectively.

Table 7 lists the different contributions to the binding free energy for the two complexes of BCD and Hexahydro-TMC 69. The values of ΔG_{bind} show that the Octyl *OH prim* conformation is slightly favored over the opposite orientation, and the corresponding, calculated values of $K_{1:1}$ (812.49 M^{-1} for Octyl *OH prim* and 825.72 M^{-1} for Octyl *OH sec*, respectively) are in good agreement with other literature data (Mura et al., 1998). Finally, the contribution of hydrophobic forces to binding is estimated to be 30.31 kJ/mol.

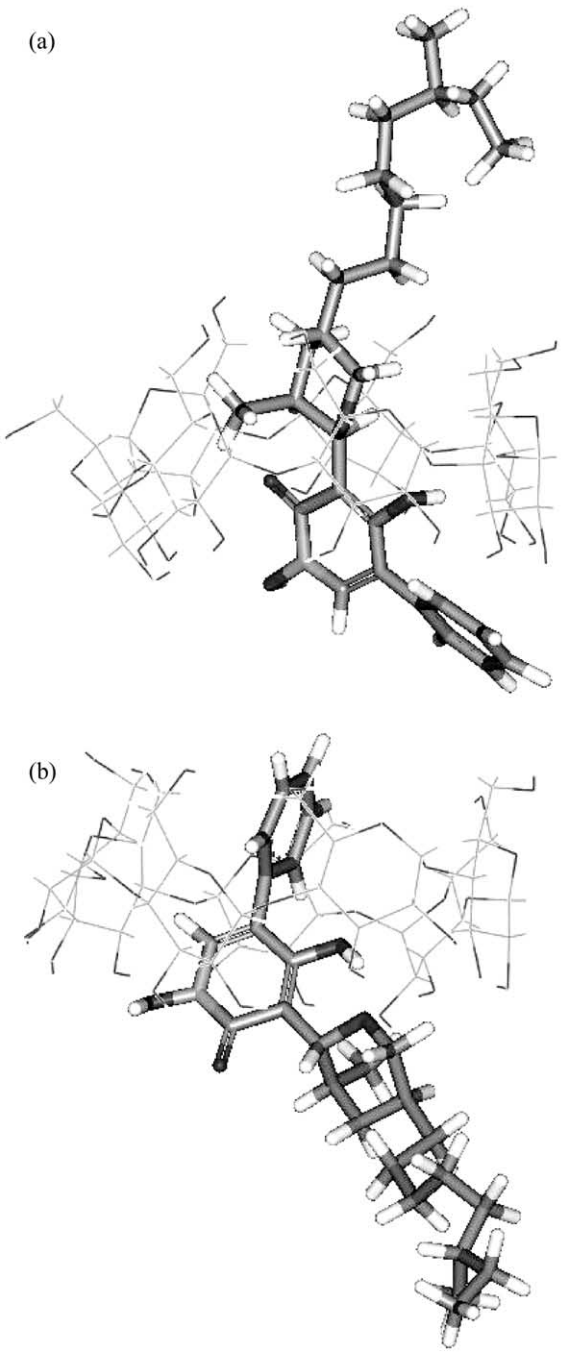

Fig. 16. Views of the equilibrium structure of the BCD–Hexahydro-TMC69 complexes after 2 ns of MD simulation: (a) Octyl *OH prim* configuration; (b) Octyl *OH sec* configuration. Water molecules have been removed for clarity.

3.4. 2:1 Complexation using explicit water solvent

Thiocolchicine and Hexahydro-TMC 69 are characterized by a very large molecular structure; thus, as already discussed in Section 3.2, the equilibrium structure complexes formed in the 1:1 stoichiometry present a relevant number of atoms of the molecule laying outside the BCD cavity. This reason, and the further evidence for a gain in

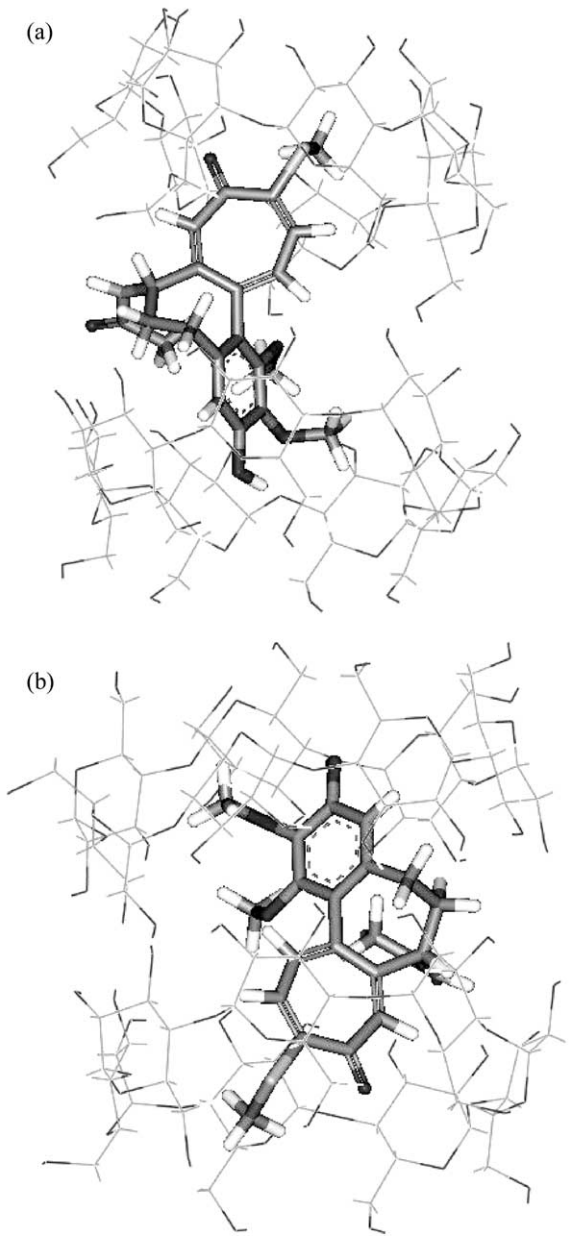

Fig. 17. Views of the equilibrium structure of the 2BCD–Thiocolchicine complexes after 2 ns of MD simulation: (a) *OH sec/OH sec* configuration; (b) *OH prim/OH sec* configuration. Water molecules have been removed for clarity.

stability for these compounds when passing to host–guest complexes characterized by a 2:1 stoichiometry, prompted us to extend the simulations to these assemblies in water.

3.4.1. 2BCD–Thiocolchicine

Fig. 17(a) and (b) shows two equilibrium conformations of the 2:1 complexes formed by Thiocolchicine with BCD, after 2 ns of MD. These snapshots give evidence of the fact that the complexes are stable, and, if compared to Fig. 15(a) and (b), we can clearly see how the drug is well wrapped by the two carbohydrate macrocycles in both cases. Furthermore, the analysis of the entire MD trajectories shows the formation of a fluctuating network of H-bonds, in particular between the two BCD molecules, which contribute to a tighter binding of the drug and to water exclusion.

The complex structure presents a drug ring in each of the BCDs; therefore, two insertion angles φ can be measured. We considered, as for the previous case, the angles φ_A related to the seven-member ring, and φ_B relative to the substituted phenyl ring. Accordingly, the average values are $\varphi_A = 96.23 \pm 7°$ and $\varphi_B = 94.56 \pm 8°$ for the *OH sec/OH sec* configuration, and $\varphi_A = 94.15 \pm 8°$ and $\varphi_B = 97.65 \pm 8°$ for the *OH prim/OH sec* configuration, respectively. The rigid characteristic of the complex structures is then well reflected by the limited variations to the average values of the corresponding insertion angles.

Table 8 reports the energetic analysis of the two complexes 2BCD–Thiocolchicine. If compared with those of 1:1 stoichiometry, the values of ΔG_{bind} for the 2:1 complexes show a significant gain in stabilization; particularly, the *OH sec/OH sec* complex, which derives from the more stable 1:1 conformation, is again more favored, also a the 2:1 stoichiometry. Interestingly enough, the calculated values of the 2:1 binding constants $K_{2:1}$, equal to 3516.61 M^{-1} for the *OH sec/OH sec*, and 2246.73 M^{-1} for the *OH prim/OH sec* configuration, respectively, are in good agreement with the values experimentally obtained for the 2:1 inclusion complex of taxol in HPBCD (Dordunoo & Burt, 1996).

The values of ΔS (12.25 kJ/mol for the *OH sec/OH sec*, and 12.01 kJ/mol for the *OH prim/OH sec* configuration, respectively) and ΔH (−7.98 and −7.11 kJ/mol) express the energetic contribution of the drug and BCD desolvation

Table 8
Energy terms and total binding free energy for 2 BCD molecules complexed-with thicolchicine and 6H-TMC69 at 310 K. All values are in kJ/mol

Contribution	ThiocolchicineOH *sec/OH sec*	Thiocolchicine *OH prim/OH sec*	6H-TMC69 *OH sec/OH sec*	6H-TMC69 *OH prim/OH sec*
ΔG_{int}^{ele}	−96.52 ± 1.22	−89.75 ± 1.01	−96.01 ± 1.20	−95.81 ± 1.12
ΔG_{int}^{vdW}	−72.48 ± 0.55	−70.55 ± 0.52	−60.11 ± 0.25	−59.48 ± 0.21
ΔG_{int}^{val}	10.26 ± 0.11	11.96 ± 0.21	14.21 ± 0.82	12.54 ± 0.73
ΔG_{MM}	−158.74 ± 1.66	−148.34 ± 1.32	−141.91 ± 0.63	−142.75 ± 0.60
ΔG_{sol}^{np}	−11.59 ± 0.08	−11.59 ± 0.08	−13.24 ± 0.09	−13.24 ± 0.09
ΔG_{sol}^{ele}	162.35 ± 2.21	152.82 ± 2.02	140.92 ± 1.98	141.31 ± 2.01
ΔG_{sol}	150.76 ± 2.13	141.23 ± 1.94	127.68 ± 1.89	128.07 ± 1.92
ΔG_{tot}^{ele}	54.24 ± 0.91	51.48 ± 0.93	31.67 ± 0.69	32.26 ± 0.80
$T\Delta S$	12.25	12.01	3.84	3.68
ΔG_{bind}	−20.23	−19.12	−18.07	−18.36

during the complexation process, and of the favorable dipole and van der Waals interactions upon binding. Accordingly, also the contribution of hydrophobic forces to binding, which can be estimated equal to 81.96 kJ/mol, assume a larger value, due to the increased number of non-polar atoms that actively interact in this system.

3.4.2. 2BCD–Hexahydro-TMC69

The underlying observations developed in Section 3.4 apply also in the case of the 2:1 Hexahydro-TMC 69 inclusion complexes. In fact, the long aliphatic chain that protrudes from the BCD cavity in the corresponding 1:1 complexes seems suitable for inclusion in a second BCD

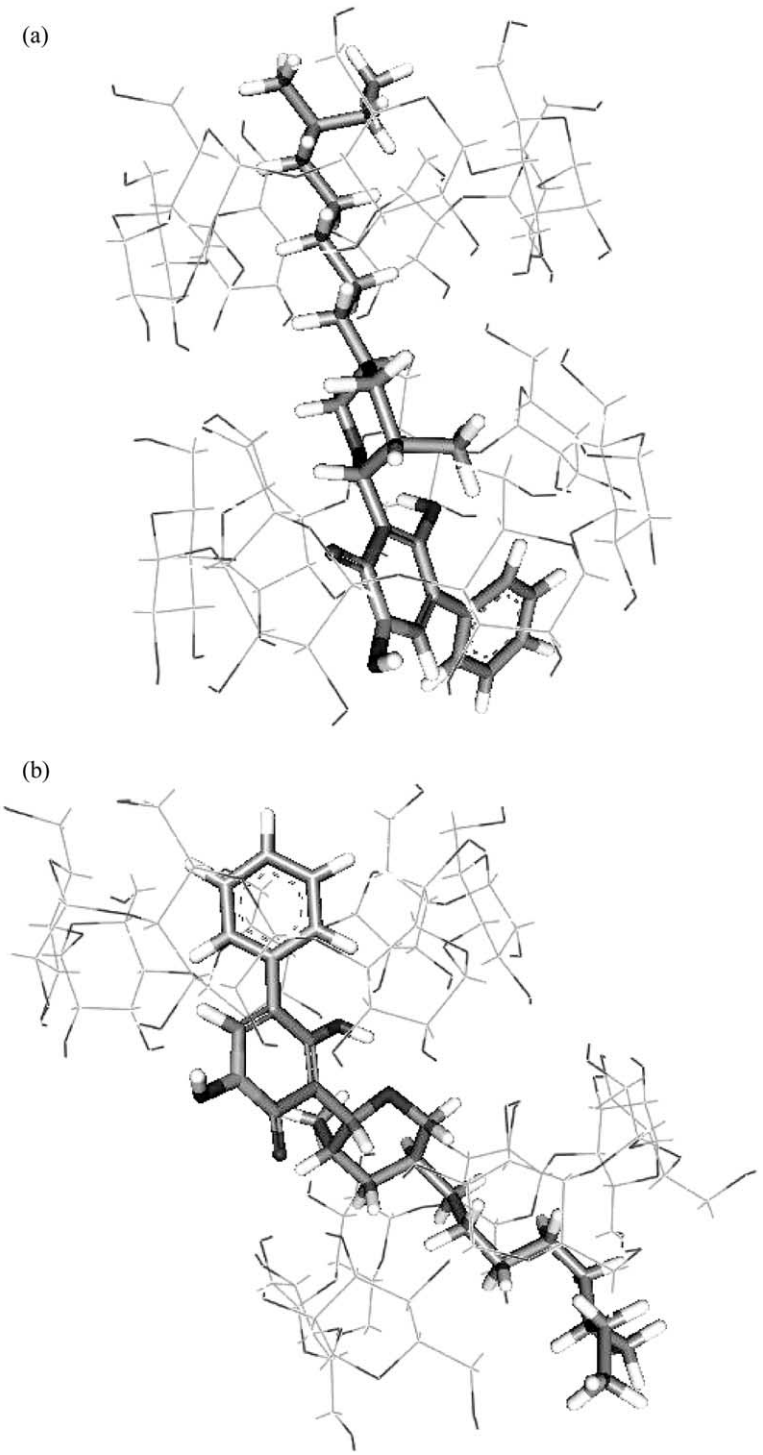

Fig. 18. Views of the equilibrium structure of the 2BCD–Hexahydro-TMC69 complexes after 400 ps of MD simulation: (a) *OH prim*/*OH sec* configuration; (b) *OH sec*/*OH sec* configuration. Water molecules have been removed for clarity.

molecule. Fig. 18 (a) and (b) shows the 2:1 equilibrium conformations of these complexes after 2 ns of MD simulation: the additional BCD molecule aptly encloses the aliphatic chain, thus creating a favorable interaction between the non-polar internal cavity of the macrocycle and the octyl chain. As for Thiocolchicine, the analysis of the entire MD trajectory reveals the presence of some unstable H-bonds, which originate almost exclusively between the two BCD molecules, thus conferring to the system a notable degree of stiffness. The last observation is supported by the limited variations of the insertion angle φ: $84.72 \pm 10°$ for the *OH sec/OH sec* configuration, and $83.97 \pm 12°$ for the *OH prim/OH sec* configuration, respectively. In addition, these values are close to those evaluated under the gas-phase simulation conditions. Finally, no water molecules were detected inside the BCD cavities during the entire simulation period.

Table 8 shows all energy terms and the binding free energy for the two complexes 2BCD–Hexahydro-TMC69. The corresponding values of values of ΔS and ΔH clearly reflect the very favorable interaction with the drug chain generated by the addition of the second BCD molecule. The same aspect contributes also to the increase in the contribution afforded by the hydrophobic forces, whose value is estimated to be equal to 81.43 kJ/mol.

As already seen for Thiocolchicine, the values of ΔG_{bind} for the 2:1 complexes are, generally speaking, more favorable than those found for the corresponding complexes in a 1:1 stoichiometry; further, in this case they are almost coincident, thus suggesting the conclusion that, for Hexahydro-TMC69, the resulting 2:1 host–guest supermolecular assembly could consist, in principle, of a mixture of the two, alternative configurations.

4. Conclusions

The more stable structures of 1:1 host–guest complexes between BCD and six anticancer drugs belonging to different classes of action were studied first by means of molecular mechanics/molecular dynamics using a continuum solvent model (GB/SA). The main driving forces for complexation are dominated by non-bonded van der Waals interactions between the host and the guest, although the relative orientation of the dipole moments and the presence of topical H-bonds between the polar parts of the drugs and the OH groups of the BCD rims play a further role in stabilizing these supermolecular assemblies. The calculations of the energetic components of the non-bonded potential energy showed that, under the conditions considered, all inclusion complexes should in principle be stable and, in the case of asymmetrical molecule, no preferential way of insertion was detected, exception made for Hexahydro-TMC69, for which the Octyl *OH prim* conformation was favored with respect to the alternative Octyl *OH sec* by approximately 18 kJ/mol.

Further, in the case of the two biggest molecules considered, Thiocolchicine and Hexahydro-TMC69, the energetical gain in the formation of 2:1 complexes was also calculated from simulation. The results clearly indicated that, under the conditions considered and in excess of BCD, the 2:1 host–guest complex stoichiometry is favored for both these two active principles. The computational results obtained so far are in good agreement with similar, published studies on BCD inclusion compounds in vacuum.

Notwithstanding this fact, the absence of an explicit solvent and the neglect of the entropic contribution does not allow for a reliable estimate of the complexation energy. Therefore, the dynamic behavior of the same 1:1 and 2:1 host–guest complexes has been simulated using a combination of molecular mechanics energy derived from MD simulations in explicit solvent, and solvation free energy derived from a continuum solvation model. Accordingly, we have calculated reasonable absolute free energies of binding for all BCD/drug complexes formation.

In general, the energetic analysis reveals that the van der Waals interactions and the non-polar contributions to solvation always provide the basis for the favorable absolute free energy of binding. On the other hand, a delicate balance exists between the always favorable gas-phase electrostatics term and the unfavorable change in electrostatic contribution to the solvation. Indeed, by counteracting the favorable electrostatic interactions that form between the drug and the BCD cavity binding site, the desolvation of the molecular components plays an important role in determining the effect of the electrostatics, as a whole, on the formation of the BCD/anticancer complexes.

The results obtained from this study can then suggest the conclusion that, although the results obtainable using continuum solvation models can be used in a predictive, comparative manner among a series of compounds, in order to investigate in detail the influence of the solvent on the interaction of the host and its guests, and to calculate reliable values for the free energy of binding, simulations in explicit water must be performed. In any case, the results we obtained by applying our simulation technique are in good agreement with published values of binding constants for analogous compounds in BCD.

Acknowledgements

Our thanks go to Jim Caldwell and the group of UCSF for providing Amber 6.0. The financial support from Italian Ministry for University and Scientific Research (MIUR, Rome, Italy, PRIN 2001 to S.P.), and from the University of

Trieste (Special Grant for Research to S.P. and M.F.) is also gratefully acknowledged.

References

Bayly, C. I., Cieplak, P., Cornell, W. D., & Kollman, P. A. (1993). *Journal of Physical Chemistry*, *97*, 10269.

Berendsen, H. J. C., Postma, J. P. M., van Gunsteren, W. F., DiNola, A., & Haak, J. R. (1984). *Journal of Chemical Physics*, *81*, 3684.

Betzel, C., Saenger, C. B., Hingerty, E., & Brown, G. M. (1984). *Journal of American Chemical Society*, *106*, 7545.

Botsi, A., Yannakopoulou, K., Hadjoudis, E., & Waite, J. (1996). *Carbohydrate Research*, *283*, 1.

Bruccoleri, R. E., Novotny, J., & Davis, M. E. (1997). *Journal of Computational Chemistry*, *18*, 268.

Case, D. A., Pearlman, D. A., Caldwell, J. W., Cheatham III, T. E, Ross, W. S., Simmerling, C. L., Darden, T. A., Merz, K. M., Stanton, R. V., Cheng, A. L., Vincent, J. J., Crowley, M., Tsui, V., Radmer, R. J., Duan, Y., Pitera, J., Massova, I., Seibel, G. L., Singh, U. C., Weiner, P. K., & Kollman, P. A (1999). *AMBER 6*, University of California, San Francisco, USA.

Choi, Y.-H., Yang, C.-H., Kim, H.-W., & Jung, S. (2000). *Carbohydrate Research*, *328*, 393.

Chong, L. T., Duan, Y., Wang, L., Massova, I., & Kollman, P. A. (1999). *Proceedings of the National Academy of Science*, *96*, 14330.

Clarke, R. J., Coates, J. H., & Lincoln, S. F. (1988). *Advances in Carbohydrate Chemistry and Biochemistry*, *46*, 205.

Connolly, M. L. (1983). *Science*, *221*, 709.

Connolly, M. L. (1985). *Journal of the American Chemical Society*, *107*, 1118.

Cornell, W. D., Cieplak, P., Bayly, C. I., Gould, I. R., Merz, K. M., Jr., Ferguson, D. M., Spellmeyer, D. C., Fox, T., Caldwell, J. W., & Kollman, P. A. (1995). *Journal of the American Chemical Society*, *117*, 5179.

Cram, D. J. (1988). *Angewandte Chemie International Edition in English*, *27*, 1009.

Darden, T., York, D., & Pedersen, L. (1993). *Journal of Chemical Physics*, *98*, 10089.

Delley, B. (1990). *Journal of Chemical Physics*, *92*, 508.

Dordunoo, S. K., & Burt, H. M. (1996). *International Journal of Pharmaceutics*, *133*, 191.

Fermeglia, M., & Pricl, S. (1999). *AIChE Journal*, *45*, 2619.

Fermeglia, M., & Pricl, S. (2001). *Carbohydrate Polymers*, *45*, 23.

Fujisawa, M., Kimura, T., & Takagi, S. (1997). *Fluid Phase Equilibrium*, *136*, 197.

Gilson, M. K., & Honig, B. H. (1988). *Proteins*, *4*, 7.

Gilson, M. K., Sharp, K. A., & Honig, B. H. (1987). *Journal of Computational Chemistry*, *9*, 327.

Griffiths, D., & Bender, M. (1973). *Advances in Catalysis*, *23*, 209.

Grigera, J. R., Caffarena, E. R., & de Rosa, S. (1998). *Carbohydrate Research*, *310*, 253.

Hirayama, F., & Uekama, K. (1999). *Advances in Drug Delivery Review*, *36*, 125.

Holland, J. F., & Frei, E., III (2000). *Cancer medicine* (5th ed). Hamilton: BC Decker Inc.

Honig, B. H., & Nicholls, A. (1995). *Science*, *268*, 1144.

Irwin, P., Brouillette, J., Giampa, A., Hicks, K., Gehring, A., & Tu, S.-I. (1999). *Carbohydrate Research*, *322*, 67.

IUPAC-IUB Commission on Biochemical Nomenclature (1970). *Journal of Molecular Biology*, *52*, 1.

IUPAC-IUB Commission on Biochemical Nomenclature (1971a). *Archives of Biochemistry and Biophysics*, *145*, 405.

IUPAC-IUB Commission on Biochemical Nomenclature (1971b). *European Journal of Biochemistry*, *18*, 151.

Ivanov, P. M., & Jaime, C. (1996). *Journal of Molecular Structure*, *377*, 137.

Jaime, C., Ridondo, J., Sanchez-Ferrando, F., & Virgili, A. (1990). *Journal of Organic Chemistry*, *55*, 4773.

Jayaram, B., Sprous, D., & Beveridge, D. L. (1998). *Journal of Physical Chemistry B*, *102*, 9571.

Jelesarov, I., Leder, L., & Bosshard, H. (1996). *Methods: Companion Methods in Enzymology*, *9*, 533.

Jiang, P., Sun, H.-W., Shen, R.-X., Shi, J., & Lai, C.-M. (2000). *Journal of Molecular Structure (Theochem)*, *528*, 211.

Jorgensen, W. L., Chandrasekhar, J., Madura, J. D., Impey, R. W., & Klein, M. L. (1983). *Journal of Computational Physics*, *79*, 926.

Katzung, B. G. (1998). *Basic and clinical pharmacology* (7th ed). Stamford, CT: Appleton & Lange.

Köhler, J. E. H., Saenger, W., & van Gusteren, W. F. (1988). *Journal of Molecular Biology*, *203*, 241.

Kohno, J., Hirano, N., Sugawara, K., Nishio, M., Hashiyama, T., Nakanishi, N., & Komatsubara, S. (2001). *Tetrahedron*, *57*, 1731.

Lindner, K., & Saenger, W. (1982). *Carbohydrate Research*, *99*, 103.

Liu, L., Li, X.-S., & Guo, Q.-X. (2000). *Journal of Molecular Structure (Theochem)*, *530*, 31.

Loftsson, T., & Brewster, M. E. (1996). *Journal of Pharmaceutical Sciences*, *85*, 1017.

Lumry, R., & Rajender, S. (1970). *Biopolymers*, *9*, 1125.

Ma, D. Q., Rajewski, R. A., & Stella, V. J. (1999). *International Journal of Pharmaceutics*, *189*, 227.

Manunza, B., Deiana, S., Pintore, M., Delogu, G., & Gessa, C. (1997). *Carbohydrate Research*, *300*, 89.

Másson, M., Loftsson, T., Jónsdóttir, S., Fridriksdóttir, H., & Petersen, D. S. (1998). *International Journal of Pharmeceutics*, *164*, 45.

Mayer, B., & Köhler, G. (1996). *Journal of Molecular Structure (Theochem)*, *363*, 217.

Menard, F. A., Dedhiga, M. G., & Rhodes, C. T. (1990). *Drug Development and Industrial Pharmacy*, *16*, 91.

Metropolis, A. W., Rosenbluth, M. N., Rosenbluth, A. H., & Teller, E. (1953). *Journal of Chemical Physics*, *21*, 1087.

Miertuš, S., Chiellini, E., Chiellini, F., Kona, J., Tomasi, J., & Solaro, R. (1999a). *Macromolecular Symposium*, *138*, 41.

Miertuš, S., Nair, A. C., Frecer, V., Chiellini, E., Chiellini, F., Solaro, R., & Tomasi, J. (1999b). *Journal of Inclusion Phenomenon and Macrocyclic Chemistry*, *34*, 69.

Misra, V. K., Sharp, K. A., Friedman, R. A., & Honig, B. H. (1994). *Journal of Molecular Biology*, *238*, 245.

Momamy, F. A., & Willett, J. L. (2000). *Carbohydrate Research*, *326*, 210.

Mura, P., Bettinetti, G. P., Manderioli, A., Faucci, M. T., Bramanti, G., & Sorrenti, M. (1998). *International Journal of Pharmaceutics*, *166*, 189.

Murphy, K., Freire, E., & Paterson, Y. (1995). *Proteins Structure Function and Genetetics*, *21*, 83.

Nesnas, N., Lou, J., & Breslow, R. (2000). *Bioorganic and Medicinal Chemistry Letters*, *10*, 1931.

Novotny, J., Bruccoleri, R. E., Davis, M., & Sharp, K. A. (1997). *Journal of Molecular Biology*, *268*, 401.

Novotny, J., & Sharp, K. A. (1992). *Progress in Biophysics and Molecular Biology*, *58*, 203.

Oh, I., Lee, M.-Y., Lee, Y.-B., Shin, S.-C., & Park, I. (1998). *International Journal of Pharmaceutics*, *175*, 215.

Pearlman, D. A., Case, D. A., Caldwell, J. W., Ross, W. S., Cheatham, T. E., III, DeBolt, S., Ferguson, D., Seibel, G. L., & Kollman, P. A. (1995). *Computers in Physics and Communication*, *91*, 1.

Raman, C., Allen, M., & Nall, B. (1995). *Biochemistry*, *34*, 5831.

Raschke, T. M., Tsai, J., & Levitt, M. (2001). *Proceedings of the National Academy of Science USA*, *98*, 5965.

Rekharsky, M. V., & Inoue, Y. (1998). *Chemical Review*, *98*, 1875.

Saenger, W., Betzel, C., Hingerty, B. E., & Brown, G. M. (1982). *Nature*, *296*, 581.

Saenger, W., Jacob, J., Gessler, K., Steiree, T., Hoffman, D., Sanbe, H.,

Koizumi, K., Smith, S.M., & Takaha, T. (1998). *Chemical Reviews*, *98*, 1787.
Sanchez-Ruiz, X., Ramos, M., & Jaime, C. (1998). *Journal of Molecular Structure*, *442*, 93.
Sanner, M. F., Olson, A. J., & Spehner, J. C. (1996). *Biopolymers*, *38*, 305.
Schwarz, F., Tello, D., Goldbaum, F., Mariuzza, R., & Poljak, R. (1995). *European Journal of Biochemistry*, *228*, 388.
Sharp, K. A. (1996). *Biophysical Chemistry*, *61*, 37.
Sharp, K. A., & Honig, B. H. (1990). *Annual Review of Biophysical Chemistry*, *19*, 301.
Shen, J., & Wendoloski, J. (1996). *Journal of Computational Chemistry*, *17*, 350.
Srinivasan, J., Cheatham, T. E., III, Cieplak, P., Kollman, P. A., & Case, D. A. (1998). *Journal of American Chemical Society*, *120*, 9401.
Sitkoff, D., Sharp, K. A., & Honig, B. H. (1994). *Journal of Physical Chemistry*, *98*, 1978.
Szente, L., & Szejtli, J. (1999). *Advances in Drug Delivery Review*, *36*, 17.
Tabushi, I., Kiyosuke, Y., Sugimoto, T., & Yamamura, K. (1978). *Journal of the American Chemical Society*, *100*, 916.
Thompson, D. O. (1997). *CRC Critical Reviews in Therapeutic Drug Carrier Systems*, *14*, 1.
Torigoe, H., Nakayama, T., Imazato, M., Shimada, I., Arata, Y., & Sarai, A. (1995). *Journal of Biological Chemistry*, *270*, 22218.
Tsumoto, K., Ogasahara, K., Ueda, Y., Watanabe, K., Yutani, K., & Kumagai, I. (1996). *Journal of Biological Chemistry*, *217*, 32612.
Uekama, K., Hirayama, F., & Irie, T. (1994). Application of cyclodextrins. Drug absorption enhancement: Concepts, possibilities, limitations and trends. In A. G. Boer (Ed.), (*Vol. 3*) (pp. 411–456). *Drug targeting delivery*, Switzerland: Harwood Academic.
Valero, M., Costa, S. M. B., Ascenso, J. R., Velázquez, M. M., & Rodríguez, L. J. (1999). *Journal of Inclusion Phenomenon and Macrocyclic Chemistry*, *35*, 663.
Velasco, J., Carmona, C., Muñoz, M. A., Guardado, P., & Balón, M. (1999). *Journal of Inclusion Phenomenon and Macrocyclic Chemistry*, *35*, 637.
Verlet, L. (1967). *Physical Review*, *159*, 98.
Weiser, J., Shenkin, P. S., & Still, W. C. (1999). *Journal of Computational Chemistry*, *20*, 217.
Wu, H (1997). *Proceedings of the First International Electronic Conference on Synthetic Organic Chemistry (ECSOC-1)*. The Internet, September 1–30, (www.mdpi.org/ecsoc/).
Yang, Z., & Breslow, R. (1997). *Tetrahedron Letters*, *38*, 6171.
Yuan, Z., Zhu, M., & Han, S. (1999). *Analytica Chimica Acta*, *389*, 291.
Zidovetzki, R., Blatt, Y., Schepers, G., & Pecht, I. (1988). *Molecular Immunology*, *25*, 205.